NASA TECHNICAL NOTE

SOUND SCATTERING BY RIGID OBLATE SPHEROIDS, WITH IMPLICATION TO PRESSURE GRADIENT MICROPHONES

Algirdas Maciulaitis, John M. Seiner, and Thomas D. Norum

Langley Research Center
Hampton, Va. 23665

NATIONAL AERONAUTICS AND SPACE ADMINISTRATION • WASHINGTON, D. C. • MAY 1976

0133829

1. Report No. NASA TN D-8140	2. Government Accession No.	3. Recipient's Catalog No.
4. Title and Subtitle SOUND SCATTERING BY RIGID OBLATE SPHEROIDS, WITH IMPLICATION TO PRESSURE GRADIENT MICROPHONES		5. Report Date May 1976
		6. Performing Organization Code
7. Author(s) Algirdas Maciulaitis, John M. Seiner, and Thomas D. Norum		8. Performing Organization Report No. L-10592
9. Performing Organization Name and Address NASA Langley Research Center Hampton, Va. 23665		10. Work Unit No. 505-03-12-02
		11. Contract or Grant No.
12. Sponsoring Agency Name and Address National Aeronautics and Space Administration Washington, D.C. 20546		13. Type of Report and Period Covered Technical Note
		14. Sponsoring Agency Code

15. Supplementary Notes

Algirdas Maciulaitis: Langley-Industry Research Associate, now at Grumman Aerospace Corporation, Bethpage, N.Y.

16. Abstract

The objective of this investigation was to determine the frequency limit below which sound scattering by a microphone body is sufficiently small to permit accurate pressure gradient measurements. To determine this limit, sound pressure was measured at various points on the surface of a rigid oblate spheroid illuminated by spherical waves generated by a point source at a large distance from the spheroid. This insured an essentially plane sound field. The measurements were made with small pressure microphones flush mounted from the inside of the spheroid model. Numerical solutions were obtained for a variety of spheroidal shapes, including that of the experimental model. Very good agreement was achieved between the experimental and theoretical results.

It was found that scattering effects are insignificant if the ratio of the major circumference of the spheroid to the wavelength of the incident sound is less than about 0.7, this number being dependent upon the shape of the spheroid. This finding can be utilized in the design of pressure gradient microphones.

17. Key Words (Suggested by Author(s)) Acoustic scattering Pressure gradient microphone Jet noise	18. Distribution Statement Unclassified — Unlimited Subject Category 71

19. Security Classif. (of this report) Unclassified	20. Security Classif. (of this page) Unclassified	21. No. of Pages 40	22. Price* $3.75

SOUND SCATTERING BY RIGID OBLATE SPHEROIDS,

WITH IMPLICATION TO PRESSURE

GRADIENT MICROPHONES

Algirdas Maciulaitis,[*] John M. Seiner,
and Thomas D. Norum
Langley Research Center

SUMMARY

The objective of this investigation was to determine the frequency limit below which sound scattering by a microphone body is sufficiently small to permit accurate pressure gradient measurements. To determine this limit, sound pressure was measured at various points on the surface of a rigid oblate spheroid illuminated by spherical waves generated by a point source at a large distance from the spheroid. This insured an essentially plane sound field. The measurements were made with small pressure microphones flush mounted from the inside of the spheroid model. Numerical solutions were obtained for a variety of spheroidal shapes, including that of the experimental model. Very good agreement was achieved between the experimental and theoretical results.

It was found that scattering effects are insignificant if the ratio of the major circumference of the spheroid to the wavelength of the incident sound is less than about 0.7, this number being dependent upon the shape of the spheroid. This finding can be utilized in the design of pressure gradient microphones.

INTRODUCTION

It has long been recognized that effective and economical suppression of undesirable noise must proceed from an adequate knowledge of the mechanism and location of noise generation. Since many noise generation problems of current interest involve very complex, spatially distributed noise sources, new analytical and experimental techniques are being developed to provide the needed acoustic data. Essentially, these techniques require synthesis of the wave vector components of an acoustic field and measurement of its spatial scale. One such technique, which has been proven useful in measuring the flux of acoustic energy from a jet, requires accurate measurement of the cross covariance of the acoustic pressure gradient (ref. 1).

[*]Langley-Industry Research Associate, now at Grumman Aerospace Corporation, Bethpage, N.Y.

There are several factors in the design of pressure gradient microphones that limit the frequency range in which accurate resolution of these pressure gradients can be obtained. Of these, consideration of the effect of scattering and diffraction by the microphone body is of prime importance and provides the motivation for the present investigation. Previous work on this problem is very limited, is almost exclusively theoretical, and deals with scattering by pressure microphones. Noteworthy contributions in this category are those of Jones (ref. 2) on the semi-infinite rod of circular cross section and of Matsui (ref. 3), who solved the same problem as Jones for more realistic boundary conditions on the face of the microphone. No previous work dealing explicitly with the scattering problem in pressure gradient microphone applications has come to the authors' attention.

Experimental determination of the upper frequency limit imposed upon a pressure gradient microphone by scattering involves several difficulties which are primarily associated with measurement of small surface pressure differences. In addition, the experimental results are also subject to imperfections in generation of a plane wave field, deviation from free-field conditions, and scattering from extraneous objects, such as the model support. It is desirable, therefore, to be able to support the experimental results, as far as possible, with exact theoretical solutions within the framework of linear acoustics.

The simplest configuration of a pressure gradient microphone is a short circular cylinder. Unfortunately, an analytical solution for the scattering about this simple shape does not exist at the present time. The closest geometrical shape for which a solution does exist is the oblate spheroid. The similarity between these two body shapes improves as the cylinder length becomes very short, which is the case of interest for pressure gradient microphones. The required analytical computation for the oblate spheroidal functions can be carried out with very high precision by utilizing computer programs recently developed at the U.S. Naval Research Laboratory (refs. 4 and 5).

In the present investigation, surface pressure distributions on a rigid oblate spheroid having major and minor axes of 25.40 cm (10.00 in.) and 8.08 cm (3.18 in.), respectively, have been measured for various sound incidence angles over the frequency range 0.200 to 3.475 kHz. In this report, the results of these measurements are presented and compared with those analytically derived. Also presented are analytical scattering pressure distributions for a zero-thickness disk and for an oblate spheroid twice as thick as the experimental model to show the effect of changing thickness. For the oblate spheroid used in the experiment, additional analytical results demonstrate the dependence of scattering on the distance between the sound source and the scatterer. Finally, scattering calculations for oblate spheroidal shapes ranging from a disk to a sphere are related to the problem of pressure gradient measurement by showing how the presence of the microphone will affect the pressure gradient of the sound field.

2

SYMBOLS

Measurements and calculations were made in U.S. Customary Units. This paper presents physical quantities in the International System of Units (SI) with the equivalent values in U.S. Customary Units given parenthetically.

A   area, m^2 (ft^2)

a   one-half of the interfocal distance (spheroid); radius (sphere and disk), m (ft)

B_{mn} coefficient in series expansion, Pa (psi)

F   frequency parameter, defined by equation (22)

g   percent of projected area

h_n spherical Bessel function

K   shape calibration factor, defined by equation (12)

k   wave number, 2π divided by wavelength, m^{-1} (ft^{-1})

m   summation index

N_{mn} normalization coefficient, defined by equation (5)

n   summation, or exponential, index

P_n Legendre polynomial

p   acoustic pressure, Pa (psi)

p_o amplitude factor of incident pressure, Pa (psi)

R_{mn} oblate spheroidal radial function

r   distance between source and field points, m (ft)

S_{mn} oblate spheroidal angular function

X,Y,Z	oblate spheroid axis system
x,y,z	Cartesian coordinates, m (ft)
α	incidence angle, deg
ϵ_m	Neumann factor, 1 when $m = 0$ and 2 otherwise
η	angular oblate spheroidal coordinate
θ	co-latitude angle in spherical coordinates, rad
ξ	radial oblate spheroidal coordinate
Π	surface pressure augmentation due to scattering, p/p_i
σ	scattering parameter, defined by equation (14)
ϕ	azimuthal oblate spheroidal coordinate, rad

Subscripts:

b	back side of body
f	front side of body
g	fraction of projected area
i	incident wave
o	source location
s	scattered wave
1	body surface

Superscripts:

(1)	first kind

4

(3)   third kind

Prime denotes derivative with respect to variable.

Bar denotes average.

EXPERIMENTAL APPARATUS

The experiment was conducted in the anechoic chamber of the National Bureau of Standards. The inside dimensions of the chamber are 10 by 6.7 by 6.7 m (33 by 22 by 22 ft). The chamber is anechoic down to 50 Hz. The test consisted of measuring the surface pressures on an oblate spheroid exposed to the harmonic sound field emanating from a 10-cm (4-in.) diameter midrange loudspeaker. The acoustic field produced by the loudspeaker was surveyed by a microphone traverse at the location where the oblate spheroid was later placed. It was found that over the frequency range of interest (0.200 to 3.745 kHz), the free-field sound pressure level across the 25.40-cm (10.00-in.) diameter of the spheroid varied by less than 0.5 dB. For the two lowest test frequencies (0.200 and 0.463 kHz), the relative variation in sound pressure level was within 0.1 dB. The distance between the loudspeaker and the oblate spheroid was 3.50 m (11.5 ft). A view of the loudspeaker and oblate spheroid model mounted inside the anechoic chamber is shown in figure 1.

Oblate Spheroid Model

The cross section of the experimental model is an ellipse having a major axis of 25.40 cm (10.00 in.), a minor axis of 8.08 cm (3.18 in.), and an interfocal distance 2a of 24.09 cm (9.48 in.). This particular shape had been selected to provide a reasonable simulation of a typical pressure gradient microphone having a thickness-to-diameter ratio of 1:4. It had been anticipated from the work of Leitner (ref. 6) and Wiener (ref. 7) that for a given body shape, scattering would be strongly dependent on the ratio of a characteristic body dimension to the wavelength of the incident sound. Therefore, the advantages of the large model size were twofold: greater accuracy in measuring surface pressure distributions and the capability to obtain meaningful scattering data at frequencies within the range of the loudspeaker and the microphones. This made it possible to use small inexpensive electret-type microphones mounted within the oblate spheroid.

The model was fabricated in two parts from an aluminum alloy. A drawing of the oblate spheroid is shown in figure 2. The two parts of the model are held together by screws from the back side, which are not shown. To keep the surface as smooth as possible, the internal microphone wells were connected to the model surface by holes 0.24 cm (3/32 in.) in diameter and 0.64 cm (1/4 in.) in depth.

Although 10 microphone wells were provided, only 1 to 7 were actually used in the experiment, and these cover a 90° angle from the axis of symmetry to the edge of the model. The other three had been originally intended for aiming the spheroid at the loudspeaker. However, this idea was later abandoned in favor of alinement with a laser beam. Because of space requirements, the two microphone holes near the thinnest part of the spheroid were not in the same azimuthal plane as the other five. Consequently, the data from these two points will not be presented other than for normal incidence.

The oblate spheroid was suspended by a 1.5-m (5.0-ft) length of 1.3-cm (1/2-in.) pipe which could be turned around its axis or adjusted vertically by means of a simple threaded device (fig. 3). This arrangement provided the means by which measurements were obtained on the surface opposite the speaker.

As shown in figure 1, 0.08-cm (1/32-in.) diameter guywires were used to insure proper alinement between the loudspeaker and the oblate spheroid. To accomplish this, a 6-mW He-Ne laser was installed in the loudspeaker holder and adjustments were made in the model suspension by observing the beam of light reflected from a small, front-surface mirror of laser quality located on the model. This mirror was adjusted prior to the test to be parallel to the diametral plane of the spheroid. In this way, the alinement accuracy of the experimental system was held within a minute of arc.

Instrumentation

Acoustic surface pressures were measured with miniature electret microphones. A general description of these microphones can be found in reference 8. The microphones were installed 0.64 cm (1/4 in.) below the model surface. The exterior dimensions of the microphone enclosure (which also housed a field effect transistor preamplifier) were 0.71 by 0.48 by 0.41 cm (0.28 by 0.19 by 0.16 in.). The frequency response of these microphones was constant within ±0.5 dB between 0.200 and 3.500 kHz. The open-circuit sensitivity, in volts per microbar, varied somewhat from microphone to microphone, ranging between -56 and -62 dB. As discussed in the following section, each microphone was carefully calibrated for each test frequency under conditions simulating the geometry of installation within the oblate spheroid.

A photograph of the inside of the spheroidal model is shown in figure 4. The microphones were held in the microphone wells by U-shaped mica retainer plates. In figure 4, the center microphone has been removed to expose the microphone hole and well. Microphones were installed with a 0.08-cm (1/32-in.) thick silicone rubber gasket sealing the periphery of the front face of the microphone. Sound pressure levels in the absence of the oblate spheroid were measured with a 1.3-cm (1/2-in.) diameter condenser microphone, whose accuracy had been calibrated with a piston-phone calibrator.

6

Equipment used during the experiments to drive the speaker and to measure acoustic pressures is schematically shown in figure 5. Microphone outputs were passed through a 10-Hz bandwidth filter and then sequentially read off from precision rms voltmeters.

Microphone Calibration

All electret-type microphones used in the experiment were calibrated for both relative and absolute sensitivity in two stages. In the first stage, relative pressure response over the working frequency range was measured by means of a cavity-type calibrator with a standard 1.3-cm (1/2-in.) condenser microphone as a reference. Microphones were mounted inside a special adapter which had been designed for insertion into the calibrator. The interior of the adapter was an exact facsimile of the microphone wells in the oblate spheroidal experimental model, including the 0.24-cm (3/32-in.) diameter by 0.64-cm (1/4-in.) long hole from the front of the microphone. This procedure established the relative sensitivity of each electret microphone.

Several problems arose in establishing an absolute sensitivity for the electret microphones. Cavity-type calibrators are sensitive to the type of microphone inserted for calibration. Since the reference and electret microphone with adapters impress a different radiation impedance in the cavity, measurement of the absolute sensitivity is subject to a small error (on the order of 1 dB in sound pressure level). Therefore, the absolute sensitivity of the electret microphones was established by a second calibration stage. A solid oblate spheroid having dimensions identical with those of the experimental model was machined to hold a standard 0.64-cm (1/4-in.) condenser microphone in the location corresponding to the central electret microphone of the model. One electret microphone was then calibrated against the 0.64-cm condenser microphone in an anechoic room at a distance of 3.50 m (11.5 ft) between the loudspeaker and the model. By using the absolute sensitivity of this microphone in conjunction with the relative sensitivity of each electret microphone, the absolute sensitivities of all microphones were determined. This procedure insured the absolute sensitivity of the electret microphones within ±0.1 dB.

ANALYTICAL FORMULATION

Coordinate System

The coordinate system relevant to the problem at hand is the oblate spheroidal system ξ, η, ϕ defined in terms of Cartesian coordinates by

$$\left. \begin{aligned} x &= a\left(1 + \xi^2\right)^{1/2}\left(1 - \eta^2\right)^{1/2} \cos \phi \\ y &= a\left(1 + \xi^2\right)^{1/2}\left(1 - \eta^2\right)^{1/2} \sin \phi \\ z &= a\xi\eta \end{aligned} \right\} \tag{1}$$

with the ranges

$$
\left.\begin{array}{l}
0 \leqq \xi < \infty \\
-1 \leqq \eta \leqq 1 \\
0 \leqq \phi \leqq 2\pi
\end{array}\right\} \tag{2}
$$

In this system, the Z-axis is the axis of symmetry; the surfaces ξ = Constant, η = Constant, and ϕ = Constant are, respectively, confocal oblate spheroids of interfocal distance 2a, confocal semihyperboloids of revolution, and semiplanes originating in the Z-axis. The limiting cases represent an infinitely thin disk (ξ = 0, a = Disk radius) and a sphere ($\xi \to \infty$, a $\to$ 0, aξ = Sphere radius). In figure 6, a sketch of the oblate spheroidal system is given, and figure 7 illustrates how the experimental model was oriented in this coordinate system.

The incidence angle α shown in figure 6 is measured from the positive Z-axis. Throughout this investigation the incidence vector is specified to lie in the X-Z plane.

The exact solutions presented in the following sections for scattering by an oblate spheroid and by a sphere can be found in reference 9 in terms of the velocity potential rather than the pressure. The assumed sinusoidal time variation is suppressed throughout the following discussion.

Point Source Solution

The incident pressure due to a point monopole source located at the position $\left(\xi_0, \eta_0, \phi_0\right)$ is given by

$$
p_i = p_0 \frac{e^{ikr}}{kr} \tag{3}
$$

where r is the distance between the source and the field point, and k is the wave number of the sound. The resulting pressure on the rigid oblate spheroid is

$$
p = \frac{2ip_0}{ka\left(1 + \xi_1^2\right)} \sum_{m=0}^{\infty} \epsilon_m \cos\left[m\left(\phi - \phi_0\right)\right] \sum_{n=m}^{\infty} \frac{R_{mn}^{(3)}\left(-ika, i\xi_0\right) S_{mn}\left(-ika, \eta_0\right) S_{mn}(-ika, \eta)}{N_{mn}(-ika) R_{mn}^{(3)'}\left(-ika, i\xi_1\right)} \tag{4}
$$

where R_{mn} and S_{mn} are oblate spheroidal radial and angular functions, respectively, and

$$
N_{mn}(-ika) = \int_{-1}^{1} \left[S_{mn}(-ika, \eta)\right]^2 d\eta \tag{5}
$$

8

Plane Wave Incidence

The incident pressure due to a plane wave traveling in the direction of the negative Z-axis is

$$p_i = p_o e^{-ikz} \tag{6}$$

The resulting pressure augmentation $\left(\Pi = p/p_i\right)$ on the surface of the rigid oblate spheroid is given by

$$\Pi = \frac{2e^{ikz}}{ka\left(1 + \xi_1^2\right)} \sum_{n=0}^{\infty} \frac{i^n S_{0n}(-ika,-1) S_{0n}(-ika,\eta)}{N_{0n}(-ika) R_{0n}^{(3)'}\left(-ika,i\xi_1\right)} \tag{7}$$

The corresponding result for a sphere with radius a is

$$\Pi = \frac{ie^{ikz}}{(ka)^2} \sum_{n=0}^{\infty} \frac{(-i)^n(2n + 1)P_n(\cos\,\theta)}{h_n^{(1)'}(ka)} \tag{8}$$

where θ is the azimuthal angle in spheroidal coordinates and P_n and h_n are the Legendre polynomial and spherical Bessel function, respectively. The derivation of equation (8) can be found in reference 10. Since the results equivalent to equations (4) and (7) are presented in reference 9 without derivation, these derivations are included for the sake of completeness in the appendix.

Effect of Scattering on the Pressure Gradient

To determine the feasibility of using a given sized body as a pressure gradient microphone, one must determine the relationship between the pressure gradient in an acoustic field and the pressure acting on the body when placed within this field. A reasonable parameter to choose is the difference in pressure acting on opposite sides of the body divided by the body thickness. The question then arises as to how well this parameter represents the pressure gradient that exists at the position of the median plane of the body when the body is removed from the field.

The difficulties involved in making this comparison can be divided into four distinguishable areas. The first arises from the fact that a gradient can never be exactly calculated from a finite difference. Since this discrepancy exists independently of the presence of the body, a term called the finite-difference factor is introduced to give an exact dependence of the pressure gradient on the free-field pressure difference.

9

The next two areas of difficulty concern differences associated with distortion of the field caused by scattering by the body surface. Even at low frequency, the pressure difference across the body will differ from that which exists over the same distance in a free field. This leads to the introduction of a so-called shape calibration constant which depends only on the shape of the body and which relates these two pressure differences. The second phenomenon due to scattering occurs at higher frequency and results in a deviation from the linear relationship between the frequency and the ratio of pressure difference to pressure gradient.

The final difficulty involves the quantization of the pressure difference across the active parts of the body. Even at low frequency, where the magnitude of the pressure is essentially uniform over the entire surface, curvature of the body results in a difference in phase at adjacent points on the body. Hence, an "average" pressure is introduced for both sides of the body. These pressures are determined by averaging the force in the gradient direction over the active portion of the body, i.e., that portion which would contain microphone sensors, and dividing by the area over which this force acts. The difference in these average pressures will be dependent on the amount of surface considered to be active. However, as will be seen later, for a given body shape, this average pressure difference divided by the distance over which it occurs is independent of the amount of active surface at all frequencies for which the body would be considered for use as a pressure gradient microphone.

To detail the discussion of pressure differences, consider a plane wave traveling in the negative z-direction, as shown in figure 8. The pressure difference between the planes $z = \Delta z/2$ and $z = -\Delta z/2$ is easily calculated from equation (6) to be

$$\Delta p_i = -2ip_o \sin\left(k\,\frac{\Delta z}{2}\right) \tag{9}$$

Since the pressure gradient at the median plane, $z = 0$, is given by

$$\left(\frac{\partial p_i}{\partial z}\right)_{z=0} = ikp_o \tag{10}$$

the relationship between the pressure difference and the pressure gradient can be expressed as

$$\frac{\Delta p_i}{\Delta z} = \left[\frac{\sin\,(k\,\Delta z/2)}{k\,\Delta z/2}\right]\left(\frac{\partial p_i}{\partial z}\right)_{z=0} \tag{11}$$

The bracketed term represents the difference between the true pressure gradient and the finite pressure difference, and was previously termed the finite-difference factor.

10

When a body of thickness Δz is placed in the field, the resulting pressure difference across the body Δp will differ from Δp_i. If a shape calibration constant K is defined as the ratio of these two differences at low frequency,

$$K = \lim_{k \to 0} \left(\frac{\Delta p_i}{\Delta p} \right)$$

(12)

equation (11) can be rewritten as

$$K \frac{\Delta p}{\Delta z} = \left[\frac{\sin (k \, \Delta z/2)}{k \, \Delta z/2} \right] \left(\frac{\partial p_i}{\partial z} \right)_{z=0}$$

(13)

Although this equation is strictly valid only in the limit of zero frequency, deviations from it will occur only after a certain frequency is attained. Below this frequency, an essentially linear relationship is seen to exist between the pressure difference across the body and the pressure gradient in the free field.

Deviations from this linearity arise at higher frequency because of two effects. First, as the frequency increases, the finite-difference factor begins to vary from its value of unity at low frequency. This merely expresses the fact that in order for a linear relationship to exist, the body thickness must be small in comparison with the wavelength of the sound, even if the body has no effect on the sound field. The second effect is due to high-frequency scattering, which causes the magnitude of the pressure on the body to be different from the magnitude of the free-field pressure. The frequency limit above which these effects become significant is investigated by introducing a scattering parameter σ:

$$\sigma = \left| \frac{\dfrac{k \, \Delta z/2}{\sin (k \, \Delta z/2)} \, K \dfrac{\Delta p}{\Delta z}}{\left(\dfrac{\partial p_i}{\partial z} \right)_{z=0}} \right|$$

(14)

This factor is chosen since by equation (13) it will be unity at low frequency.

The value of the shape calibration constant and the behavior of the scattering parameter can be determined for the oblate spheroid. For a plane sound wave traveling in the direction normal to the major axis of the spheroid (fig. 9), the average pressure difference across the body is calculated in the manner previously indicated. For any arbitrary percentage g of projected area, the average pressure acting on the front side of the spheroid is

11

$$\bar{p}_f = \frac{\int_{A_g} p \, dA}{\int_{A_g} dA} \qquad (15)$$

where dA is an element of projected area and A_g is the total area of interest. Since an element of projected area on the spheroid $\xi = \xi_1$ is given by

$$dA = 2\pi a^2 \left(1 + \xi_1^2\right) \eta \, d\eta \qquad (16)$$

this average pressure becomes

$$\bar{p}_f = \frac{2}{1 - \eta_g^2} \int_{\eta_g}^{1} p(\eta) \eta \, d\eta \qquad (17)$$

where η_g is the value of η that encloses the area A_g, and is easily shown to be

$$\eta_g = \left(1 - \frac{g}{100}\right)^{1/2} \qquad (18)$$

After the average pressure on the corresponding area on the back side of the spheroid $\bar{p}_b$ is computed in the same way, the pressure difference across the spheroid is calculated from

$$\Delta p = \bar{p}_f - \bar{p}_b \qquad (19)$$

The body thickness corresponding to this difference in average pressure is computed in the same manner and is given by

$$\Delta z = 2 \frac{\int_{A_g} z \, dA}{\int_{A_g} dA} = \frac{4a\xi_1 \left(1 - \eta_g^3\right)}{3\left(1 - \eta_g^2\right)} \qquad (20)$$

From equations (10) and (19), the scattering parameter defined by equation (14) can be written

12

$$\sigma = \left| \frac{K}{2 \sin (k \, \Delta z/2)} \left(\frac{\bar{p}_f - \bar{p}_b}{p_0} \right) \right| \qquad (21)$$

For the oblate spheroid, the body pressure and thickness can be computed from equations (17) and (20), respectively.

Note that equation (21) can be used for two purposes. First, the shape calibration constant K can be determined from the fact that the scattering parameter σ must equal unity at low frequency. Second, the frequency limit can be found by noting the variation of the scattering parameter with a frequency parameter. Above this limit the pressure difference across the spheroid is no longer simply related to the pressure gradient. The frequency parameter is conveniently chosen to be equal to the ratio of the body circumference (normal to the wave) to its wavelength, which for the oblate spheroid is

$$F = ka \left(1 + \xi_1^2 \right)^{1/2} \qquad (22)$$

Computer Programs

The oblate spheroidal functions needed in the calculation of the pressure distribution on the spheroid were obtained from modifications of the computer programs described in references 4 and 5. The computed results were determined to an accuracy of at least five significant figures. Computations were performed on a Control Data (CDC) 6600 computer system.

DISCUSSION OF RESULTS

As a preliminary check of the validity of the computing program, a comparison was made with the results of Leitner (ref. 6). This comparison is for a plane wave incident on a disk, which is the limiting case of an oblate spheroid. It is apparent from figure 10, where the pressure augmentations calculated from equation (7) are plotted, that the agreement with Leitner's computations is excellent, except in the region near the edge of the disk. The small differences near the edge of the disk are probably due to the greater accuracy in the present investigation, which was made possible by the extremely accurate subroutines for oblate spheroidal functions taken from references 4 and 5. Also shown in the figure are Wiener's (ref. 7) experimental results. These differ from the calculated results for two reasons: the finite thickness of the disk used in the experiment; and experimental errors, partly caused by an external probe microphone used to measure surface pressures.

Comparison of Experimental and Analytical Results

The experiment was performed at frequencies from 0.200 to 3.475 kHz, corresponding to a range of frequency parameter F from 0.455 to 7.911. The model was turned both to change the incidence angle and, since all pressure taps were located on one face of the model, to measure the surface pressure on the back side. The experimentally determined surface pressure distributions are shown in figures 11 to 14. Also included in these figures are the theoretically predicted values, as computed from equation (4). The results presented are for five values of the frequency parameter F (0.455, 1.055, 2.110, 4.219, and 7.911) and four incidence angles α (180°, 150°, 120°, and 90°). The ordinate Π in these plots is termed the surface pressure augmentation due to scattering and is computed as the ratio of the rms value of the pressure at a given point on the surface of the oblate spheroid to the value at that point in the absence of the spheroid. With the exception of the data on the back side of the model at α = 150°, the agreement between experimental and analytical results is seen to be very good. The reasons for the disagreement at α = 150° have not been found; unfortunately, it was not feasible to repeat this portion of the experiment.

As seen in figures 11 to 14, only a small amount of scattering is present at the lowest test frequency (F = 0.455). At higher frequencies the change in the pressure distribution around the spheroid ranges from a very drastic one at α = 180° to almost a uniform small increase in pressure for α = 90°. It should be kept in mind that the pressure distributions shown are for one particular plane through the spheroid — only that normal to the X-axis.

It is interesting to note that for α = 180° (fig. 11), both theory and experiment indicate a pressure augmentation greater than a factor of 2 on the front of the spheroid at F = 2.110. As the frequency is increased further, the peak values of Π approach 2, as one would expect. Figures 11(d) and 11(e) show that the pressure can peak at locations off the center line and that more than one "loud spot" can occur on the back side. The latter finding, which is analogous to the diffraction ring pattern in optics, is not unexpected.

Pressure Distributions in the X-Z Plane for Oblate Spheroids

The experimental data were obtained essentially in a single plane normal to the X-axis (see fig. 7), which for arbitrary plane wave incidence provides only a partial picture of the scattering effects. A more complete picture of these effects is given in figure 15, which shows the calculated surface pressure augmentation in the X-Z plane at the same source positions and frequencies as in the experiments.

These results were computed from equation (4) and are plotted in polar form against the argument $\cos^{-1} \eta$. For incidence at 180° and 90°, where the pressure distributions

are symmetrical, only one-half of the distribution is shown. It should be noted that the results for $F = 0.455$ (fig. 15(a)) are plotted on an enlarged scale.

One can note from these figures that whenever a loud spot exists on the back side of the spheroid, it occurs almost exactly opposite the incident wave direction. However, the pressure peaks on the front side can be found far removed from the incident direction. Figure 15(a) indicates that scattering does not appreciably alter the surface pressure distribution at low frequency.

Variation of Π With Distance Between Source and Model

The computed results plotted in figures 16(a) and 16(b) show how the surface pressure augmentation would vary for the oblate spheroid model $\left(\xi_1 = 0.336\right)$ used in the experiment for different distances between the loudspeaker and the model. In these calculations the sound source was assumed to lie on the Z-axis. The pressure augmentations for a separation distance of 35.0 m (115 ft) are essentially identical with those for plane wave incidence. It is apparent from these graphs that the distance used in the experiment, 3.50 m (11.5 ft), provided results very close to those for plane wave incidence. As the frequency increases, the small differences that do exist become progressively smaller, as can be observed by comparing figures 16(a) and 16(b).

Effects of Doubling the Oblate Spheroid Thickness

Calculated surface pressure augmentations for the experimental model and for a model having twice the thickness $\left(\xi_1 = 0.826\right)$ are compared in figures 17(a) and 17(b). These calculations are based on a sound source at $\alpha = 180^O$ and $r = 35.0$ m (115 ft). As expected, figure 17(a) demonstrates that the thickness of the body has little effect on the surface pressure distribution at low frequency; but at higher frequency (fig. 17(b)), the scattering effects become strongly dependent upon the geometrical shape.

Effects of Scattering on Pressure Gradient Measurements

One important consideration must be stressed before making inferences about the effects of scattering on pressure gradient microphones. All results obtained in the course of the present investigation, both experimentally and analytically, are for "hard" bodies, i.e., bodies with infinite acoustic impedance on their surface. Therefore, the findings presented are applicable either to microphones with very high impedance, such as the piezoelectric and piezoresistive types, or to those in which the active portions constitute a small fraction of the otherwise hard casing surface.

By the use of equation (21) for low frequency where $\sigma = 1$, the shape calibration factor K was determined for the entire range of oblate spheroids from a disk to a sphere. These results are presented in figure 18 as a function of the ratio of minor to

major diameters of the spheroid. Note that K is always less than unity, which means that the pressure difference across the spheroid is always larger than the pressure difference that would exist over the same distance in the absence of the spheroid.

After the value of the shape calibration constant was determined, equation (21) was used to compute the variation of the scattering parameter σ with frequency. For the particular oblate spheroid used in the experiment, the scattering parameter is plotted against the frequency parameter F in figure 19. Results are shown for three choices of the percent of projected area over which the average pressure is computed. As can be observed, the scattering parameter is essentially independent of the percent of projected area up to F = 1.0. A similar result was found for the sphere and other oblate spheroids.

A useful feature of these results can be seen in figure 20. Here the scattering parameter is plotted against F for several oblate spheroidal shapes. As can be observed, the useful frequency range over which a body can be used to measure the free-field pressure gradient accurately is highly dependent upon the geometrical shape of the body. For example, in measurement of the pressure gradient within a relative error of ±1 dB (±12.2 percent), the results indicate that the high-frequency limit for a disk is approximately only four-tenths of that for the oblate spheroid with $\xi = 0.826$. As shown in figure 20, the disk represents the geometrical shape most sensitive to scattering effects. For this shape, incident wavelengths should be confined to values of F < 0.7 to obtain a relative error less than ±1 dB.

CONCLUDING REMARKS

Acoustic pressure distributions have been measured on the surface of a rigid 25.40- by 8.08-cm (10.00- by 3.18-in.) oblate spheroid in a harmonic plane wave field under anechoic conditions. Numerical solutions have been generated for the first time both to provide comparisons with experimental results and to investigate different oblate spheroidal shapes. Good agreement between experimental and analytical results has been obtained.

The findings in this investigation indicate that pressure gradient microphones having oblate spheroidal shapes – all the way from a disk to a sphere – will be relatively free from scattering effects as long as the ratio of the major circumference of the body to the wavelength of the sound is kept below about 0.7. This information allows the selection of the proper size and shape for a spheroidal-shaped microphone in any intended frequency range. It was also found that below the frequency limit set by scattering considerations, the determination of the pressure gradient is dependent on the particular microphone geometry. This dependence must be either analytically or experimentally determined.

Since pressure gradient microphones are usually constructed in the shape of short circular cylinders, it is recommended that future scattering experiments using large models be extended to include such shapes. It is further suggested that in future work, small microphones be mounted flush with the model surface to avoid some of the calibration difficulties encountered in the present work.

Langley Research Center
National Aeronautics and Space Administration
Hampton, Va. 23665
March 30, 1976

APPENDIX

SOLUTION OF THE WAVE EQUATION IN TERMS OF
OBLATE SPHEROIDAL FUNCTIONS

Solution for Point Source

The oblate spheroidal coordinate system allows an exact solution of the linearized wave equation. Although the solution for the pressure applicable to the scattering problem for oblate spheroids follows a standard procedure and the final result is given in reference 9, a step-by-step derivation could not be found in the literature and is therefore included herein for the sake of completeness.

In brief, the solution involves the series expansion of the pressure of the incoming wave in terms of radial and angular oblate spheroidal functions and trigonometric functions. Another series expansion containing undetermined coefficients is then assumed for the scattered wave. In this expansion the radial functions of the third kind are specified, since they represent outgoing waves. The undetermined coefficients are evaluated by means of the boundary condition at the body surface $\partial p/\partial \xi = 0$ at $\xi = \xi_1$, which states that the normal velocity is zero at the surface of the rigid spheroid.

Suppression of the time variation allows the incident pressure due to a point source located at (ξ_0, η_0, ϕ_0) to be determined by equation (3). When the incoming wave is expanded in terms of the functions of interest, equation (3) becomes (see ref. 10)

$$p_i = 2ip_0 \sum_{m,n} \frac{\epsilon_m}{N_{mn}(-ika)} S_{mn}(-ika,\eta) \, S_{mn}\left(-ika,\eta_0\right) R_{mn}^{(1)}(-ika,i\xi)$$

$$\times R_{mn}^{(3)}\left(-ika,i\xi_0\right) \cos\left[m\left(\phi - \phi_0\right)\right] \tag{A1}$$

where $R_{mn}^{(1)}$ is the radial oblate spheroidal function of the first kind and the other terms have been previously defined.

Specifying the pressure due to the scattered wave as

$$p_s = \sum_{m,n} B_{mn} \, S_{mn}(-ika,\eta) \, R_{mn}^{(3)}(-ika,i\xi) \cos\left[m\left(\phi - \phi_0\right)\right] \tag{A2}$$

and using the boundary condition gives

$$B_{mn} = \frac{-2i\epsilon_m p_o}{N_{mn}(-ika)} \frac{R_{mn}^{(1)'}\left(-ika, i\xi_1\right) R_{mn}^{(3)}\left(-ika, i\xi_o\right)}{R_{mn}^{(3)'}\left(-ika, i\xi_1\right)} S_{mn}\left(-ika, \eta_o\right) \qquad (A3)$$

The pressure existing at any point on or outside the spheroid $\xi = \xi_1$ is then the sum of the incident and scattered pressures. On the surface of the spheroid, this addition yields

$$p = \frac{2ip_o}{ka\left(1 + \xi_1^{\,2}\right)} \sum_{m,n} \frac{\epsilon_m \, S_{mn}(-ika, \eta) \, S_{mn}\left(-ika, \eta_o\right)}{N_{mn}(-ika)} \frac{R_{mn}^{(3)}\left(-ika, i\xi_o\right)}{R_{mn}^{(3)'}\left(-ika, i\xi_1\right)} \cos\left[m\left(\phi - \phi_o\right)\right] \qquad (A4)$$

where use of the Wronskian for the radial functions (ref. 10), which can be written as

$$R_{mn}^{(1)}\left(-ika, \xi_1\right) R_{mn}^{(3)'}\left(-ika, \xi_1\right) - R_{mn}^{(3)}\left(-ika, \xi_1\right) R_{mn}^{(1)'}\left(-ika, \xi_1\right) = \frac{1}{ka\left(1 + \xi_1^{\,2}\right)} \qquad (A5)$$

has been used.

Solution for Plane Wave Traveling in Negative z-Direction

The incident pressure due to a plane wave traveling in the negative z-direction is given by equation (6). Expanding this in terms of the spheroidal functions yields (ref. 10)

$$p_i = 2p_o \sum_{n=0}^{\infty} \frac{i \, S_{0n}(-ika, -1) \, S_{0n}(-ika, \eta) \, R_{0n}^{(1)}(-ika, i\xi)}{N_{0n}(-ika)} \qquad (A6)$$

The pressure due to the outgoing scattered wave is again expanded in terms of the radial functions of the third kind as

$$p_s = \sum_{n=0}^{\infty} B_{0n} \, S_{0n}(-ika, \eta) \, R_{0n}^{(3)}(-ika, i\xi) \qquad (A7)$$

APPENDIX

The coefficients are evaluated as for the point source by the specification of zero pressure gradient normal to the body surface. Proceeding in the same manner as for the point source leads to the result

$$p = \frac{2p_o}{ka\left(1 + \xi_1^{\,2}\right)} \sum_{n=0}^{\infty} \frac{i^n \, S_{0n}(-ika, -1) \, S_{0n}(-ika, \eta)}{N_{0n}(-ika) \, R_{0n}^{(3)\,'}\left(-ika, i\xi_1\right)} \tag{A8}$$

at all points on the surface of the spheroid $\xi = \xi_1$.

20

REFERENCES

1. Maestrello, Lucio: On the Relationship Between Acoustic Energy Density Flux Near the Jet Axis and Far-Field Acoustic Intensity. NASA TN D-7269, 1973.

2. Jones, D. S.: The Scattering of a Scalar Wave by a Semi-Infinite Rod of Circular Cross Section. Phil. Trans. Roy. Soc. London, ser. A, vol. 247, no. 934, April 19, 1955, pp. 499-528.

3. Matsui, E.: On the Free-Field Correction for Laboratory Standard Microphones Mounted on a Semi-Infinite Rod. NBS Rep. 7038, Dec. 1960.

4. King, B. J.; and Van Buren, A. L.: A Fortran Computer Program for Calculating the Prolate and Oblate Angle Functions of the First Kind and Their First and Second Derivatives. NRL Rep. 7161, U.S. Navy, Nov. 30, 1970.

5. Van Buren, A. L.; Baier, R. V.; and Hanish, S.: A Fortran Computer Program for Calculating the Oblate Spheroidal Radial Functions of the First and Second Kind and Their First Derivatives. NRL Rep. 6959, U.S. Navy, Jan. 20, 1970. (Available from DDC as AD 722 649.)

6. Leitner, Alfred: Diffraction of Sound by a Circular Disk. J. Acoust. Soc. America, vol. 21, no. 4, July 1949, pp. 331-334.

7. Wiener, Francis M.: The Diffraction of Sound by Rigid Disks and Rigid Square Plates. J. Acoust. Soc. America, vol. 21, no. 4, July 1949, pp. 334-347.

8. Sessler, G. M.; and West, J. E.: Electret Transducers: A Review. J. Acoust. Soc. America, vol. 53, no. 6, June 1973, pp. 1589-1600.

9. Bowman, J. J.; Senior, T. B. A.; and Uslenghi, P. L. E., eds.: Electromagnetic and Acoustic Scattering by Simple Shapes. John Wiley & Sons, Inc., 1969, pp. 511-514.

10. Morse, Philip M.; and Ingard, K. Uno: Theoretical Acoustics. McGraw-Hill Book Co., Inc., c.1968.
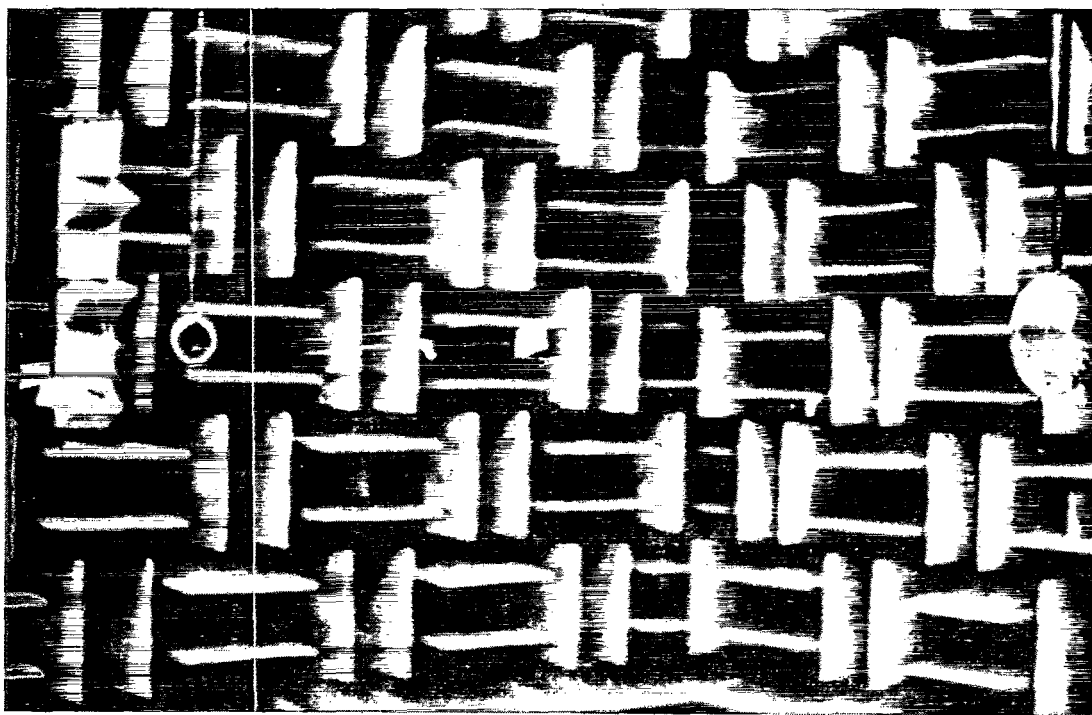
L-76-158

Figure 1.- Loudspeaker and model inside National Bureau of
Standards anechoic chamber.

22
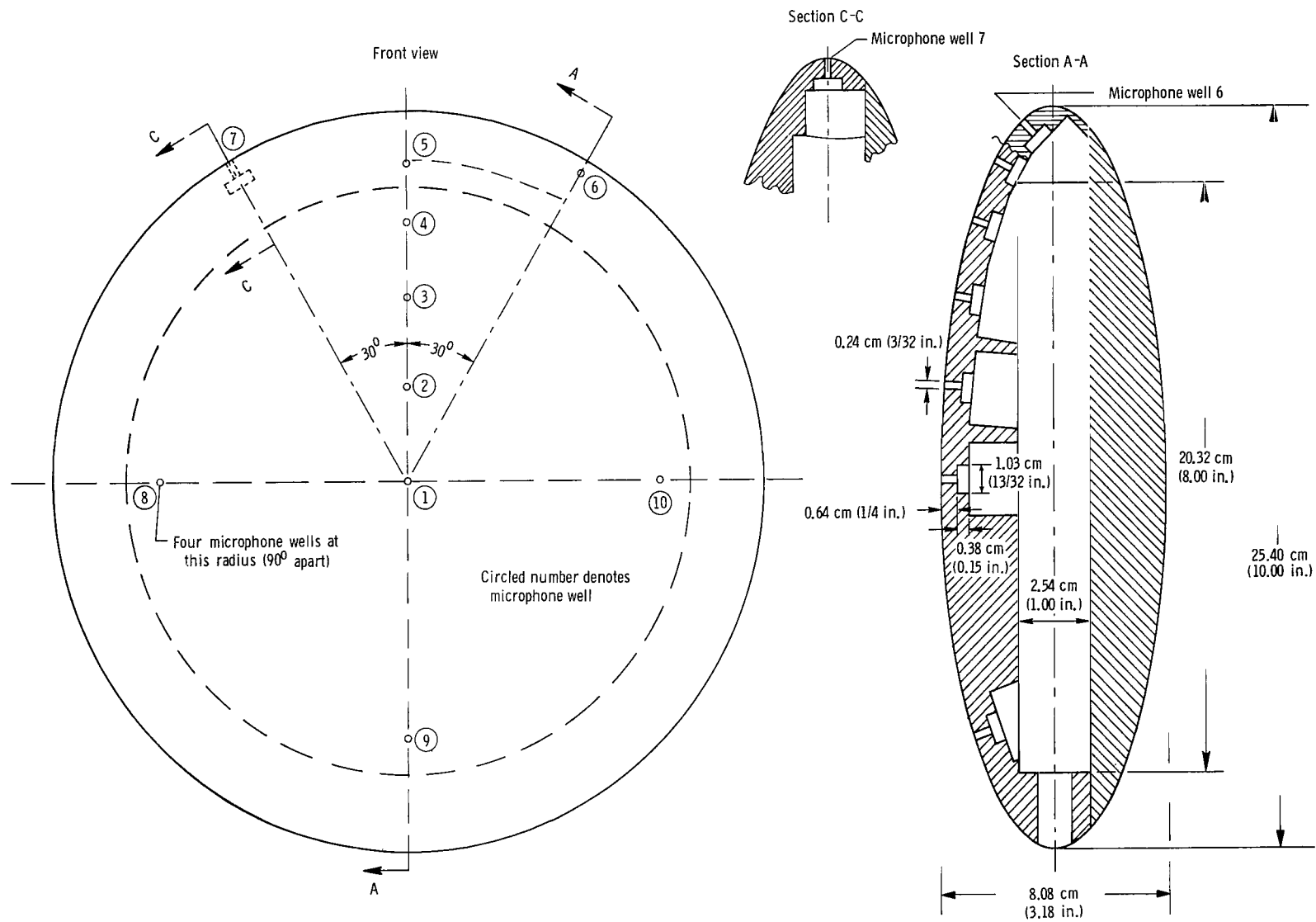
Figure 2.- Experimental model.
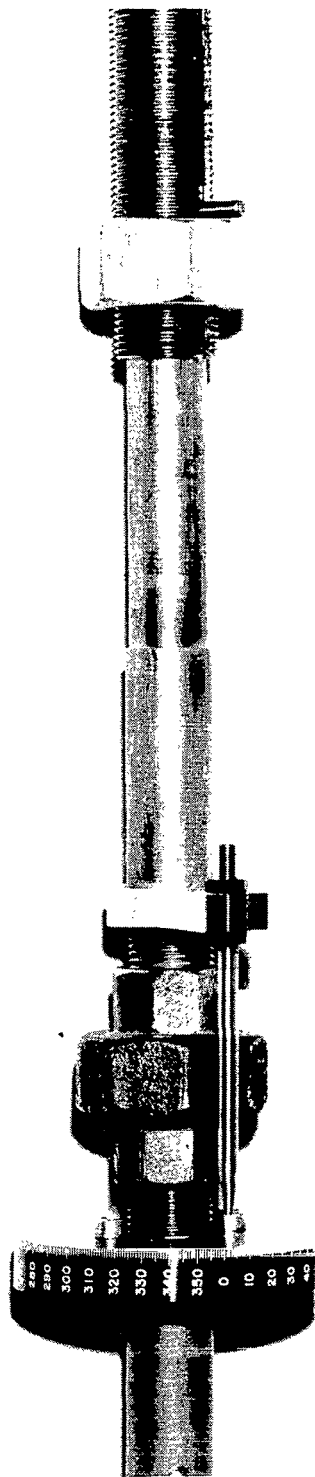
L-75-4339

Figure 3.- Model positioner.
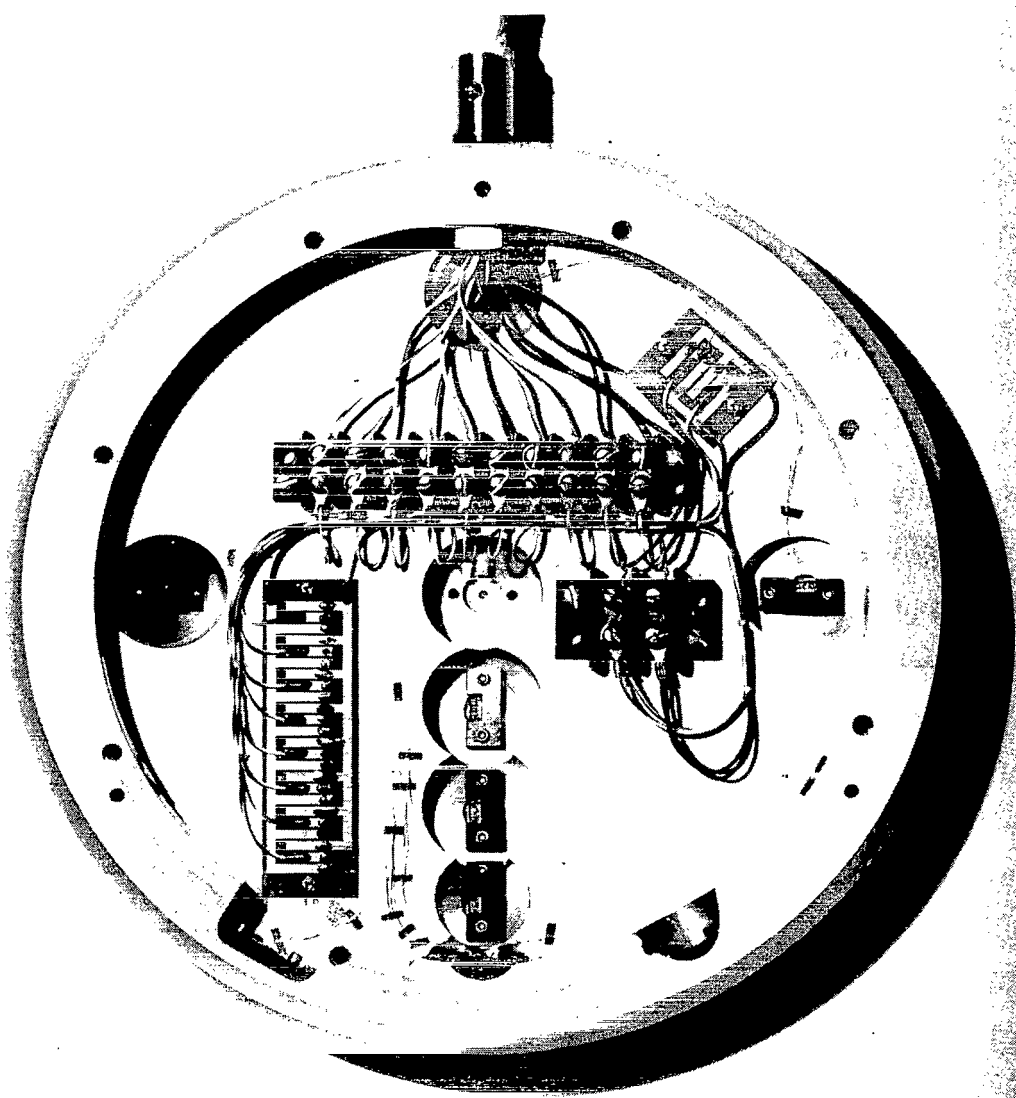
Figure 4.- Inside view of experimental model.

OBLATE SPHEROID

SPEAKER

ELECTRET MICROPHONES

1/2-in.
MICROPHONE

POWER SUPPLY

JUNCTION BOX
AND
POWER SUPPLY

POWER
AMPLIFIER

SWEEP
OSCILLATOR

FREQUENCY
COUNTER

DYNAMIC
ANALYZER
FILTER

SWITCHING
BOX

VOLTMETER

LOW-NOISE
rms
VOLTMETER

OSCILLOSCOPE

LOW-NOISE
rms
VOLTMETER
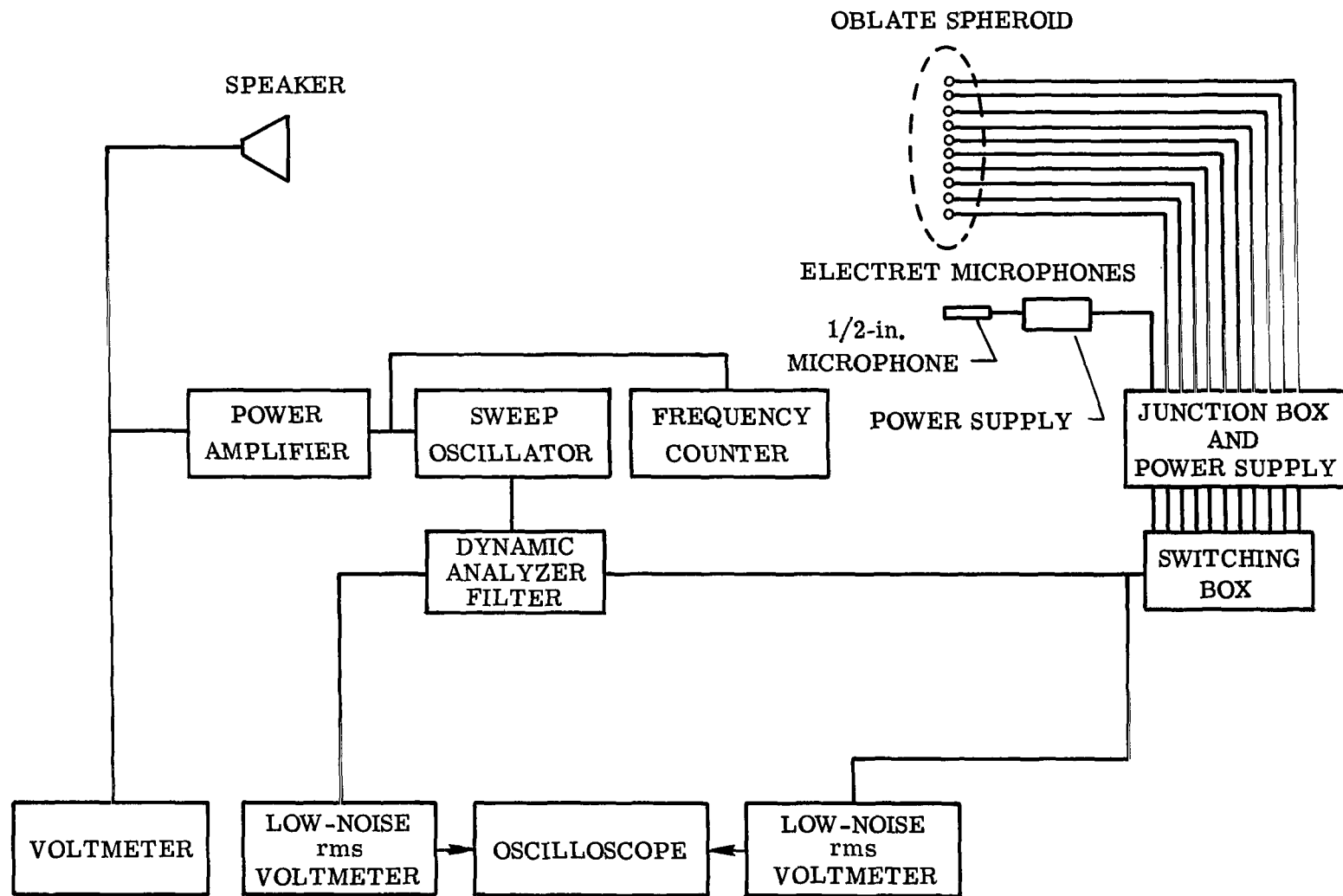
Figure 5.- Block diagram of experimental setup.
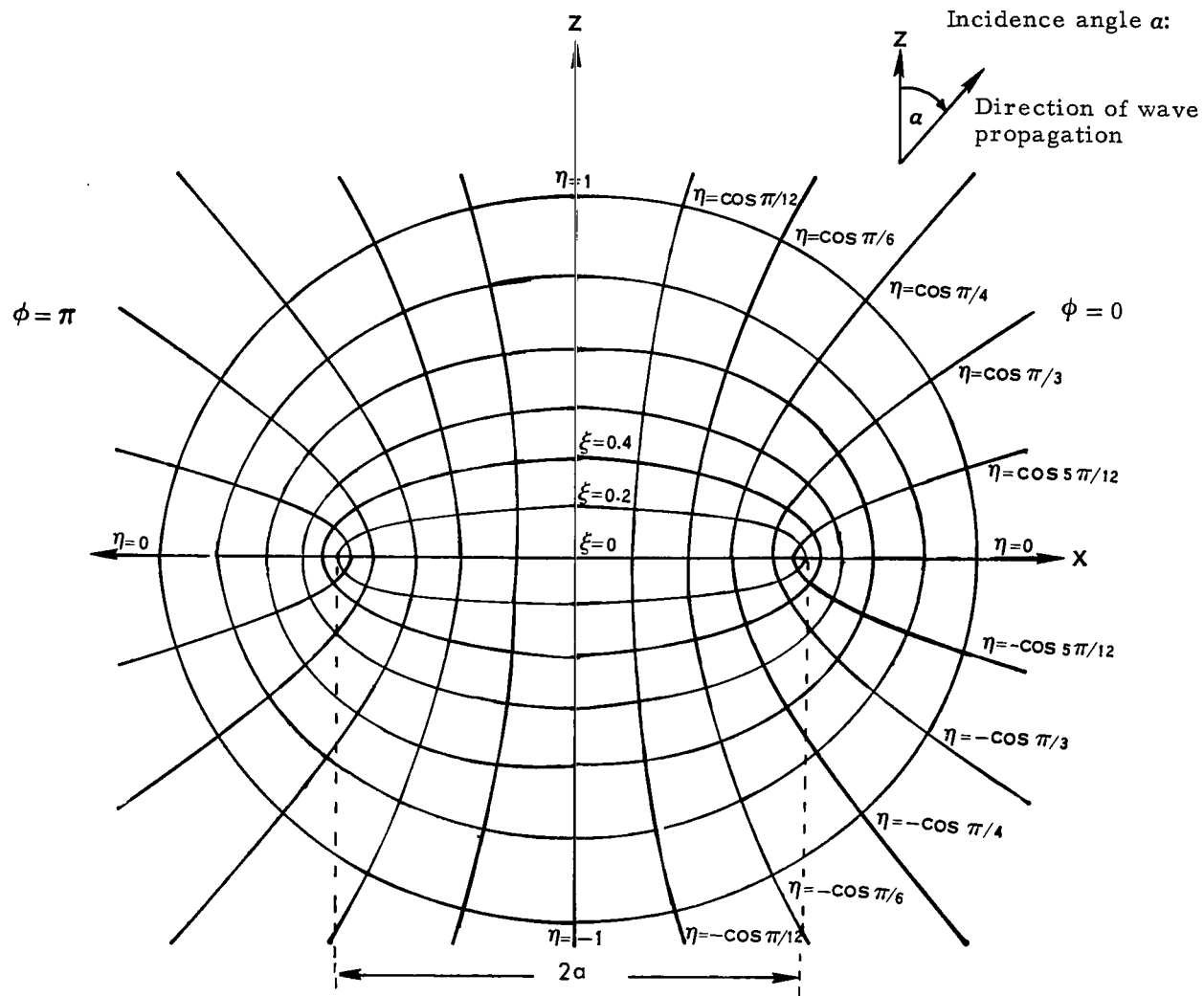
Figure 6.- Oblate spheroidal coordinate system.

Support and
axis of rotation

Oblate spheroid model

Focus

$\xi_1 = 0.336$

a

$\eta = 1.0$

Z

$\eta = \cos \pi/12$

$\eta = \cos \pi/6$

$\eta = \cos \pi/4$

$\eta = \cos \pi/3$

Y

Microphone locations

Loudspeaker
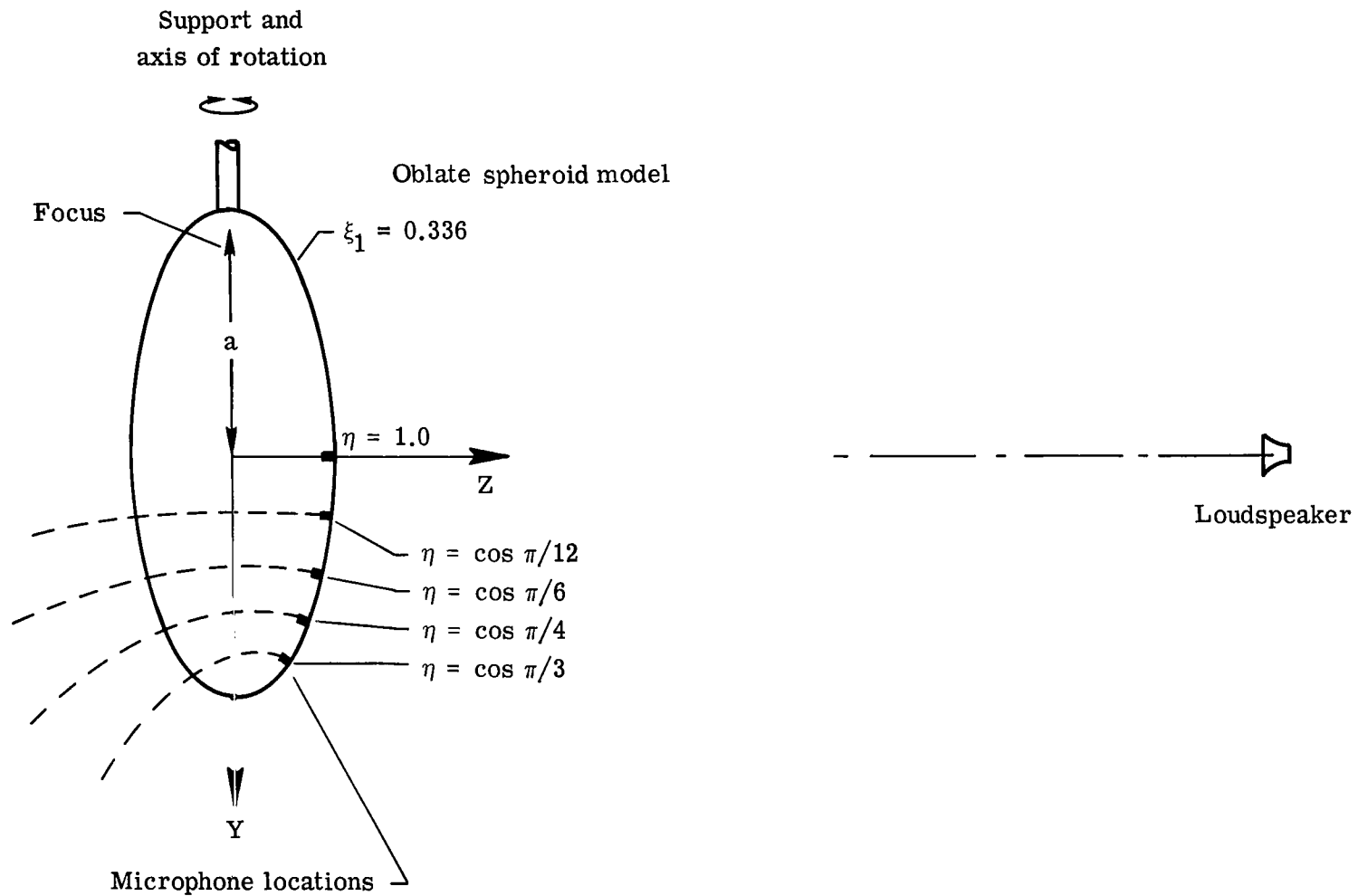
Figure 7.- Side view of experimental setup in terms of oblate spheroidal
coordinate system for 180° incidence.

$$p_i = p_o e^{-ikz}$$

$$\downarrow \quad \downarrow \quad \downarrow \quad \downarrow \quad \downarrow$$

Free-field plane wave

$$p_i = p_o e^{-ikz}$$

$$\downarrow \quad \downarrow \quad \downarrow \quad \downarrow \quad \downarrow$$

Incident plane wave

Z

$$z = \frac{\Delta z}{2}$$

X

$$\Delta z$$

$$z = -\frac{\Delta z}{2}$$
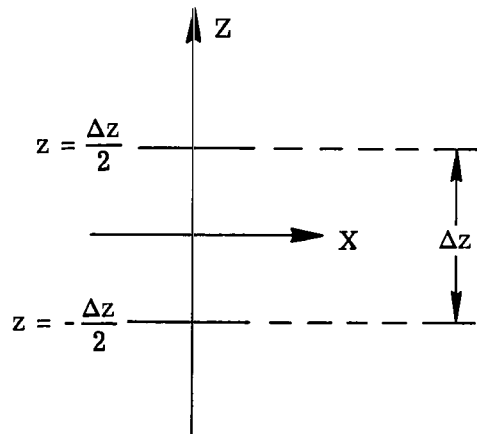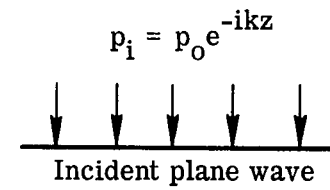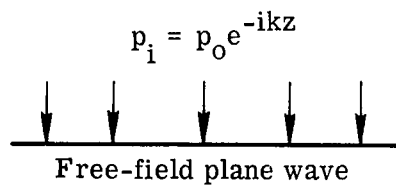
Figure 8.- Plane wave in free field.

Z

Area A_g over which averaging is done

$$\eta = \eta_g$$

$$\Delta z$$

X

Spheroid surface $\xi = \xi_1$

$$\eta = -\eta_g$$
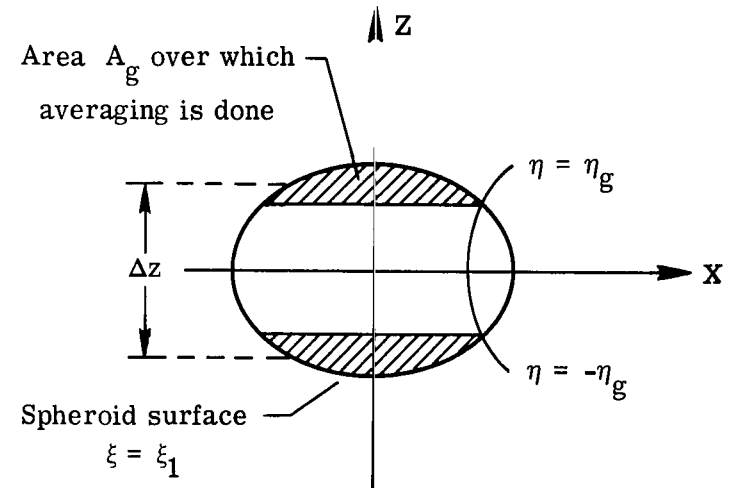
Figure 9.- Plane wave incident on the oblate spheroid $\xi = \xi_1$.
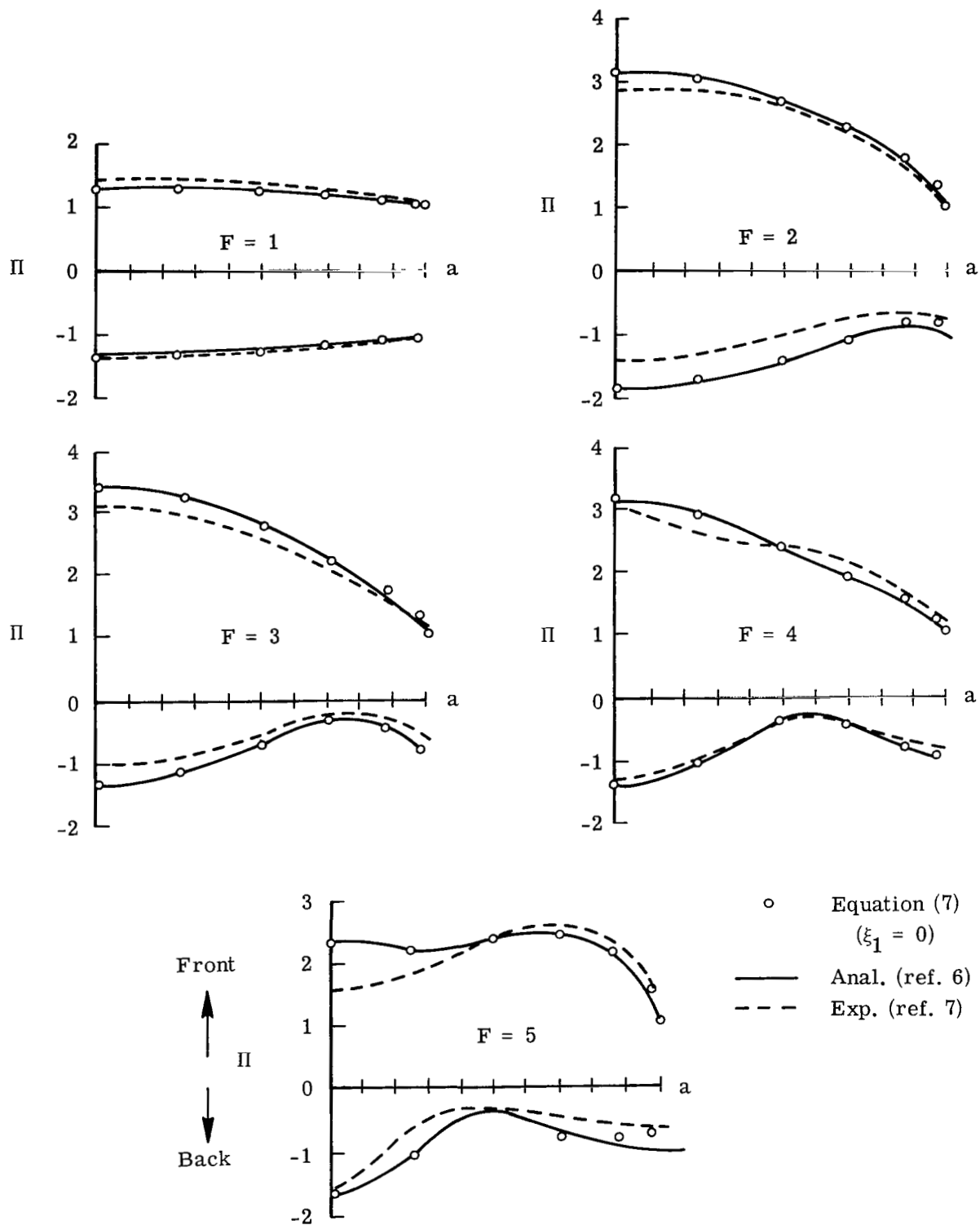
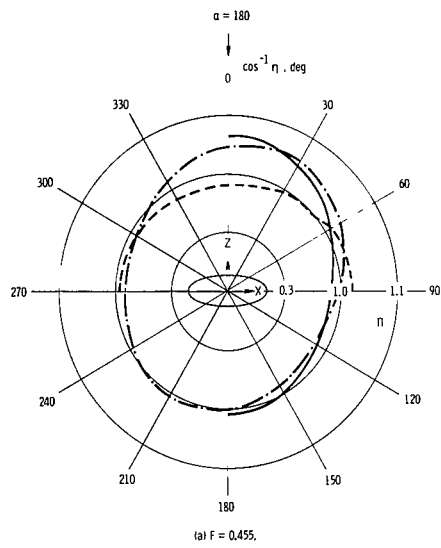Figure 10.- Surface pressure augmentation on disk with radius   a.
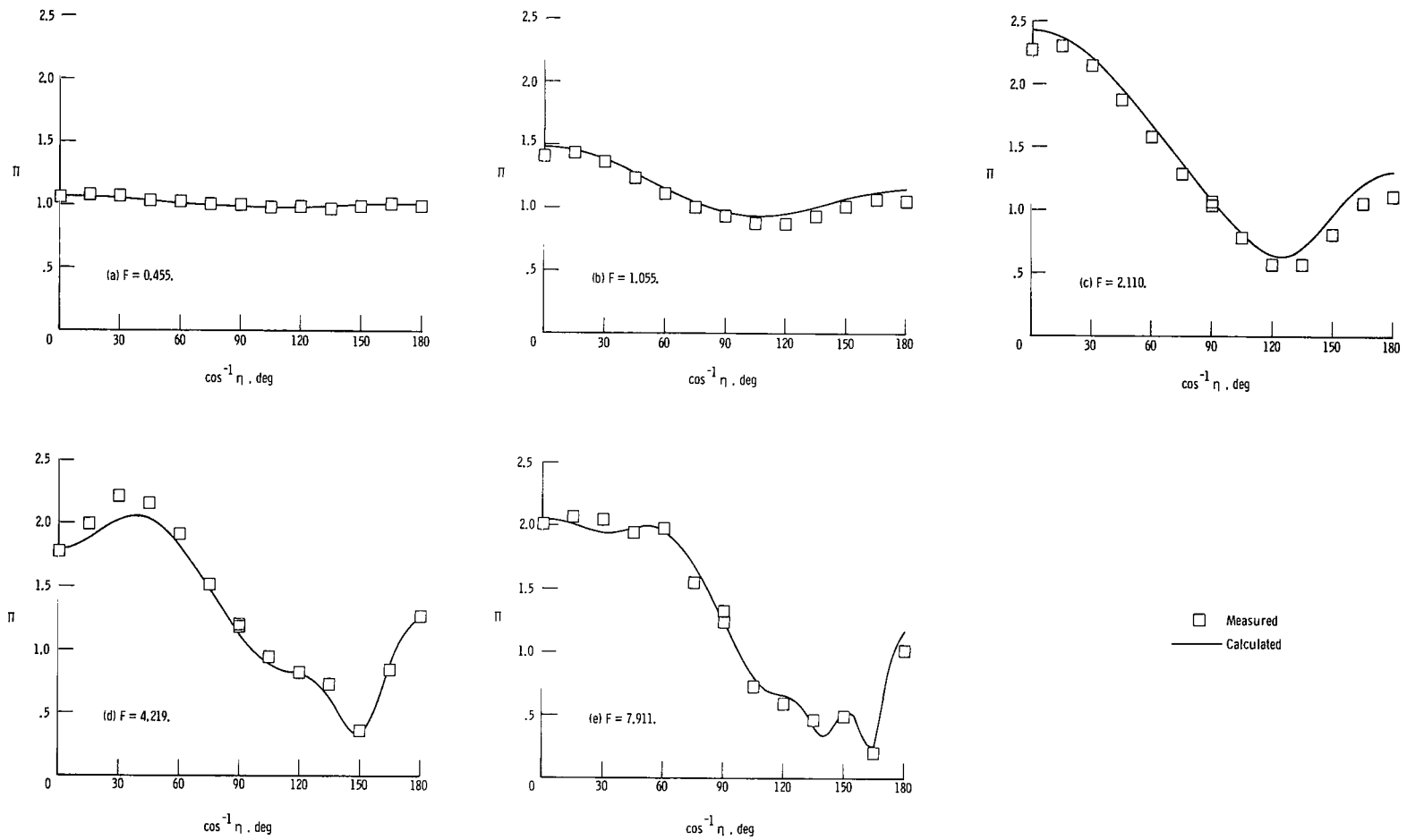
Figure 11.- Comparison of measured and calculated surface pressure augmentation due to scattering for 180° incidence to the oblate spheroid $\xi_1 = 0.336$.
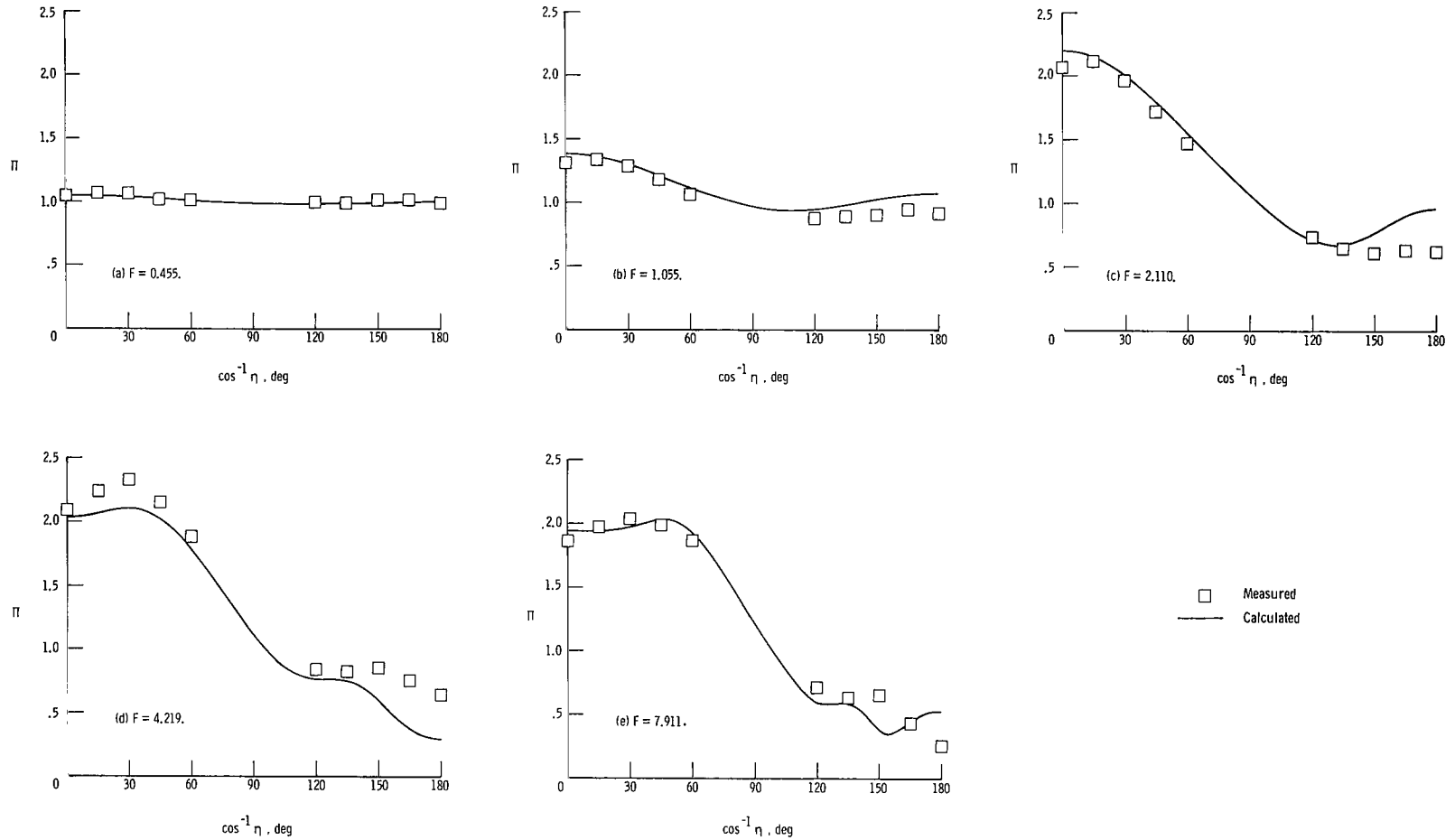
Figure 12.- Comparison of measured and calculated surface pressure augmentation due to scattering for 150° incidence to the oblate spheroid $\xi_1 = 0.336$.
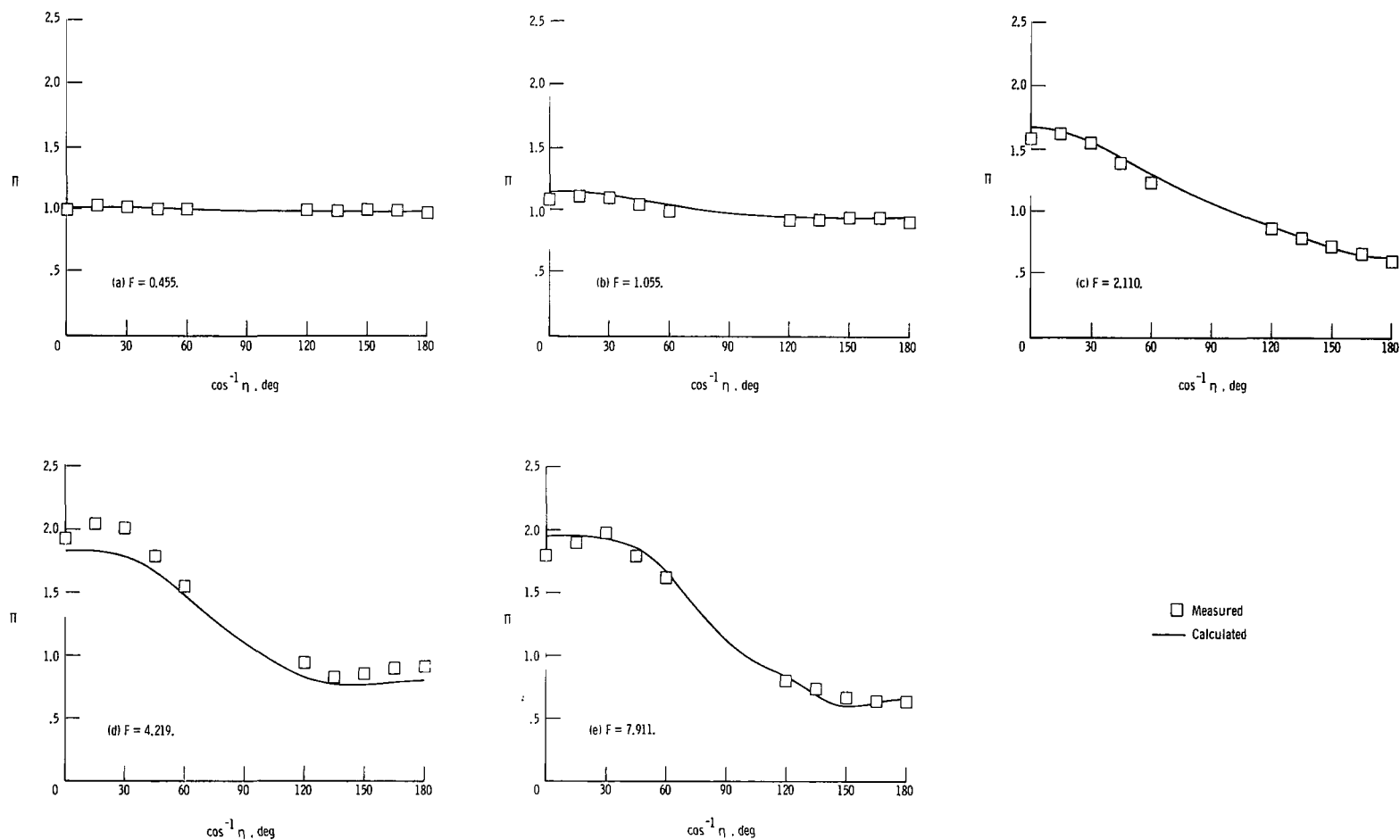
Figure 13.- Comparison of measured and calculated surface pressure augmentation due to scattering for 120° incidence to the oblate spheroid $\xi_1 = 0.336$.
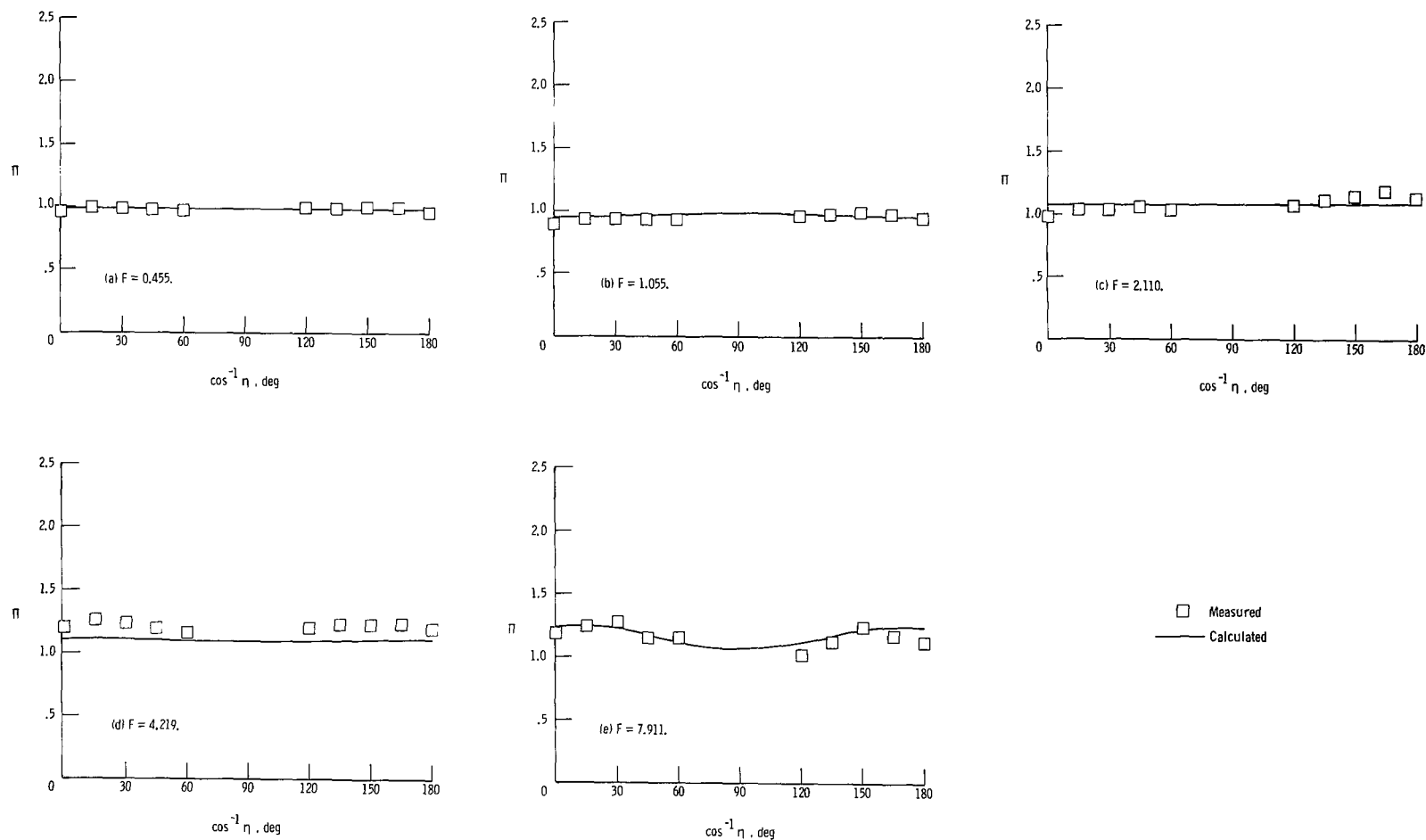
Figure 14.- Comparison of measured and calculated surface pressure augmentation due to scattering for 90° incidence to the oblate spheroid $\xi_1 = 0.336$.
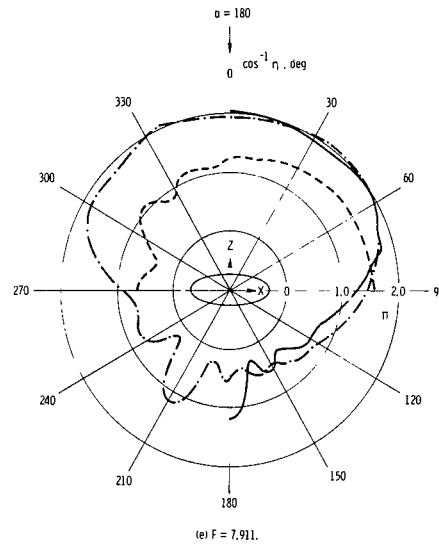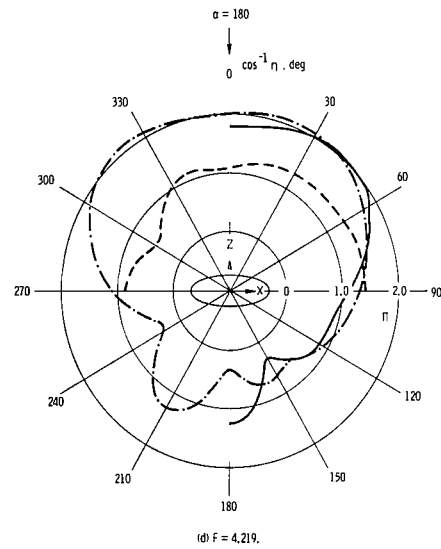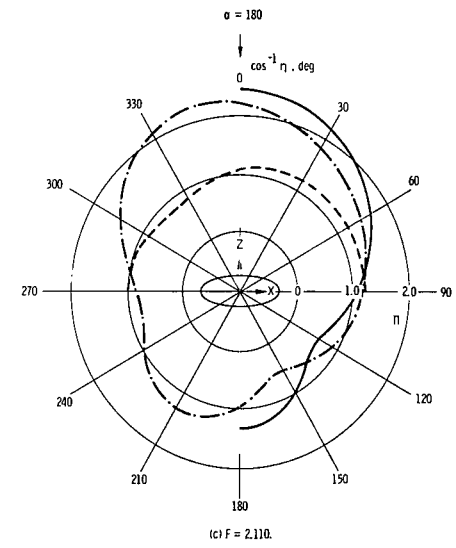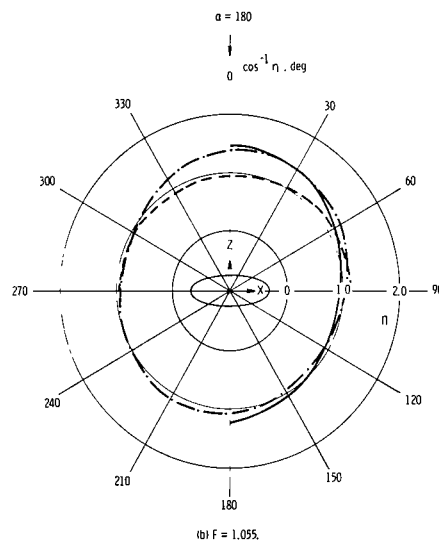
Figure 15.- Surface pressure augmentation due to scattering in the
X-Z plane of the oblate spheroid $\xi_1 = 0.336$.
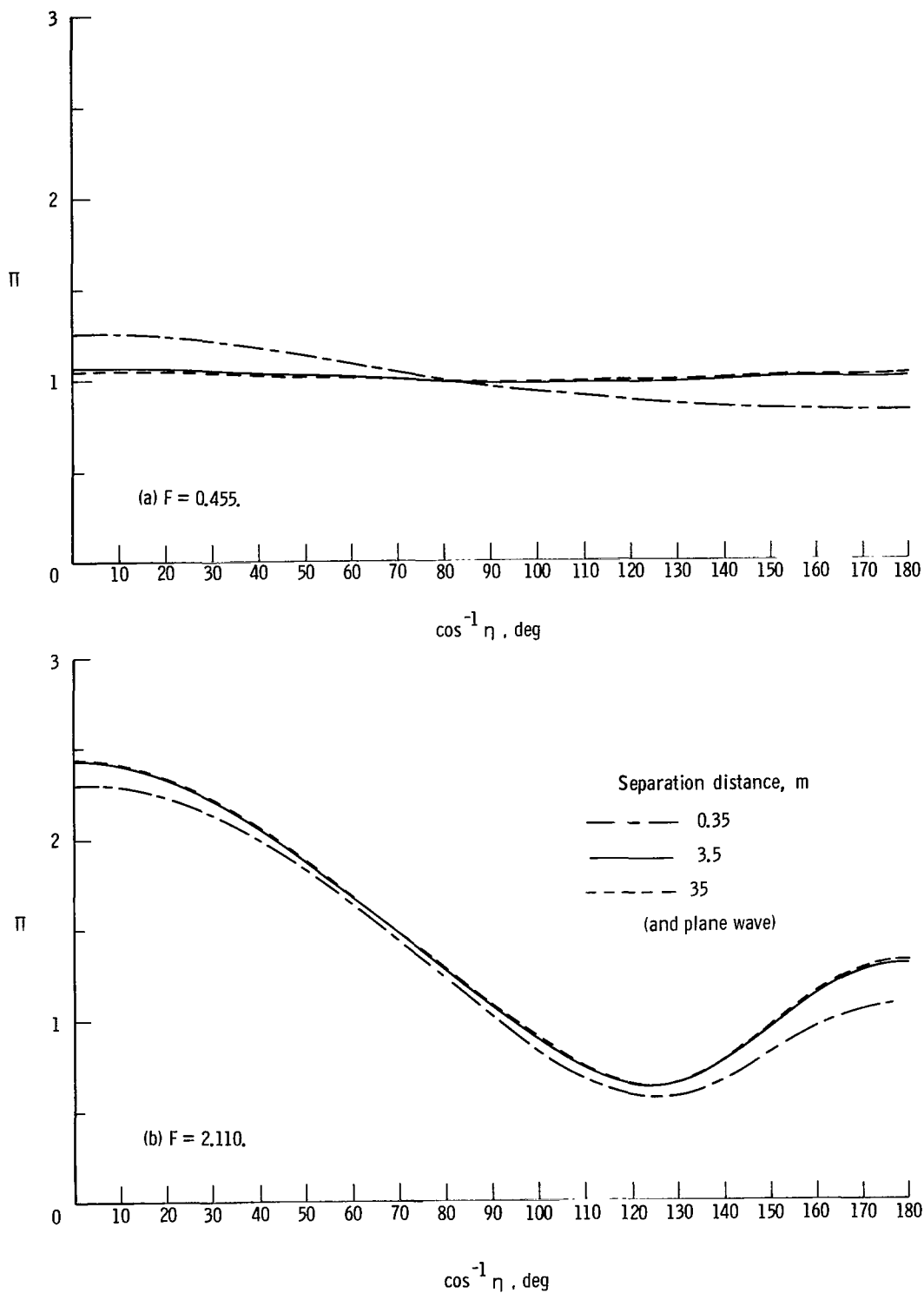
Figure 16.- Dependence of surface pressure augmentation on distance between point source and the oblate spheroid $\xi_1 = 0.336$. $\alpha = 180^\circ$.
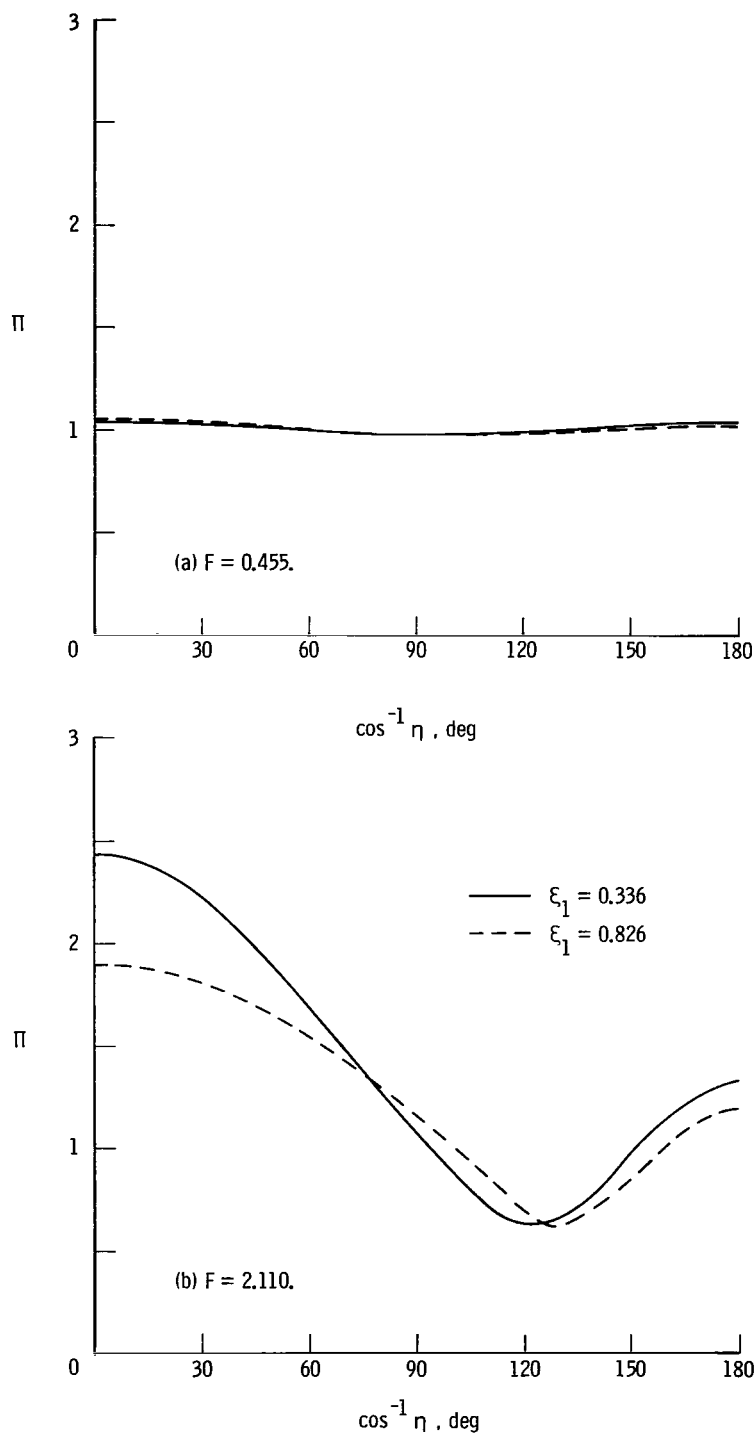
Figure 17.- Comparison of surface pressure augmentation due to
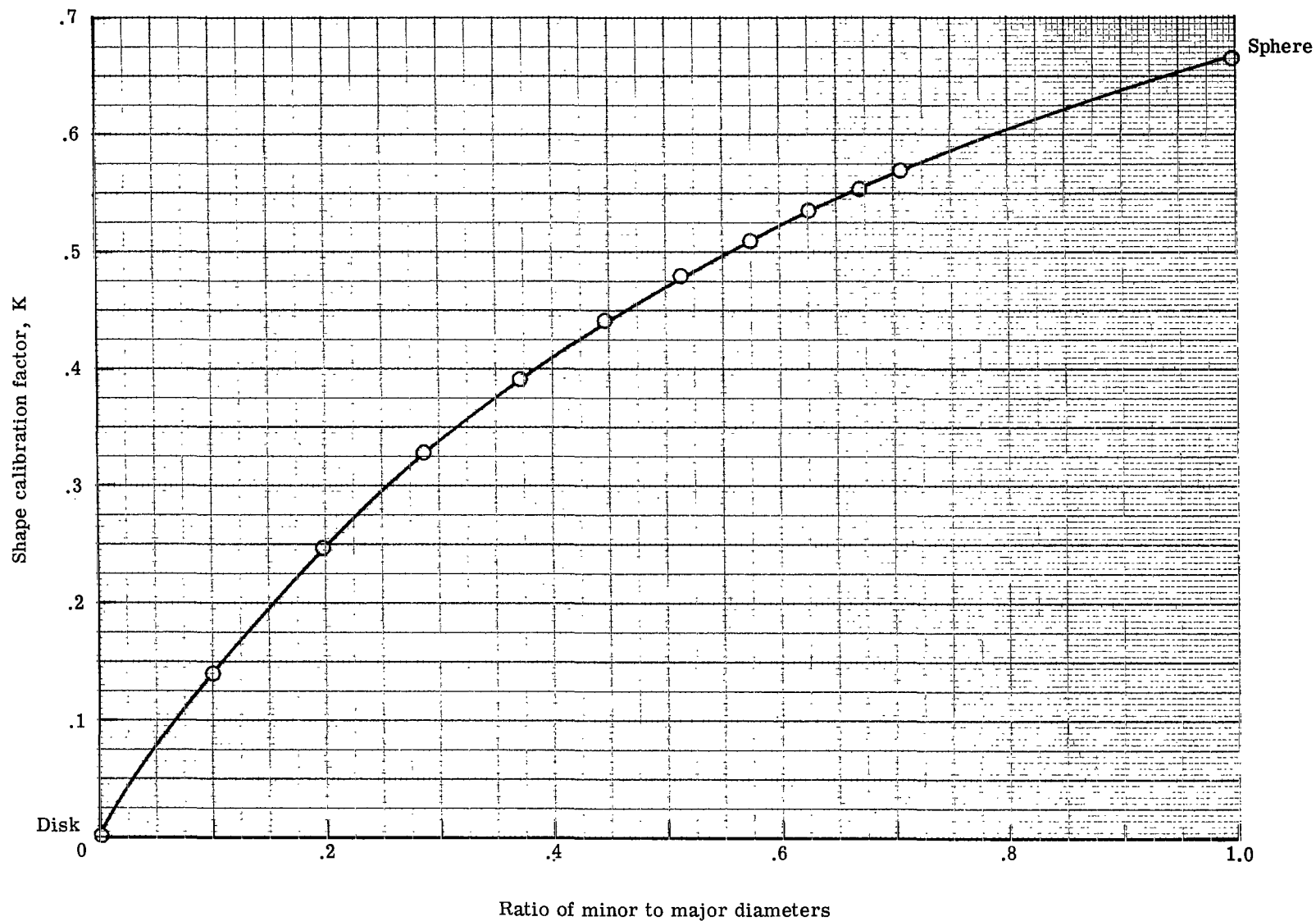scattering for two oblate spheroids. $\alpha = 180^O$.

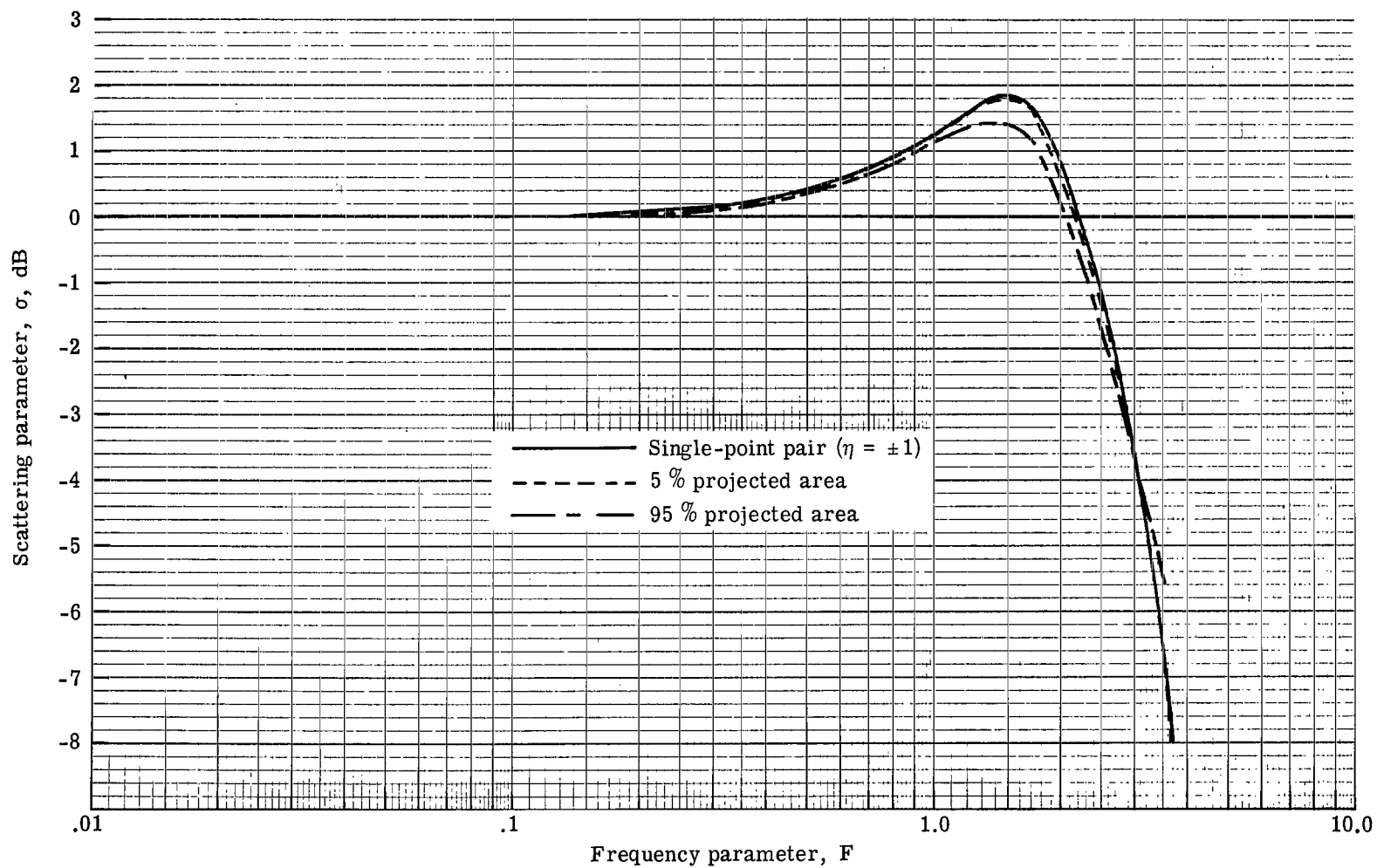Figure 18.- Shape calibration constant for all oblate spheroids.

Figure 19.- Variation of scattering factor with frequency parameter for several projected areas. $\xi_1 = 0.336$.
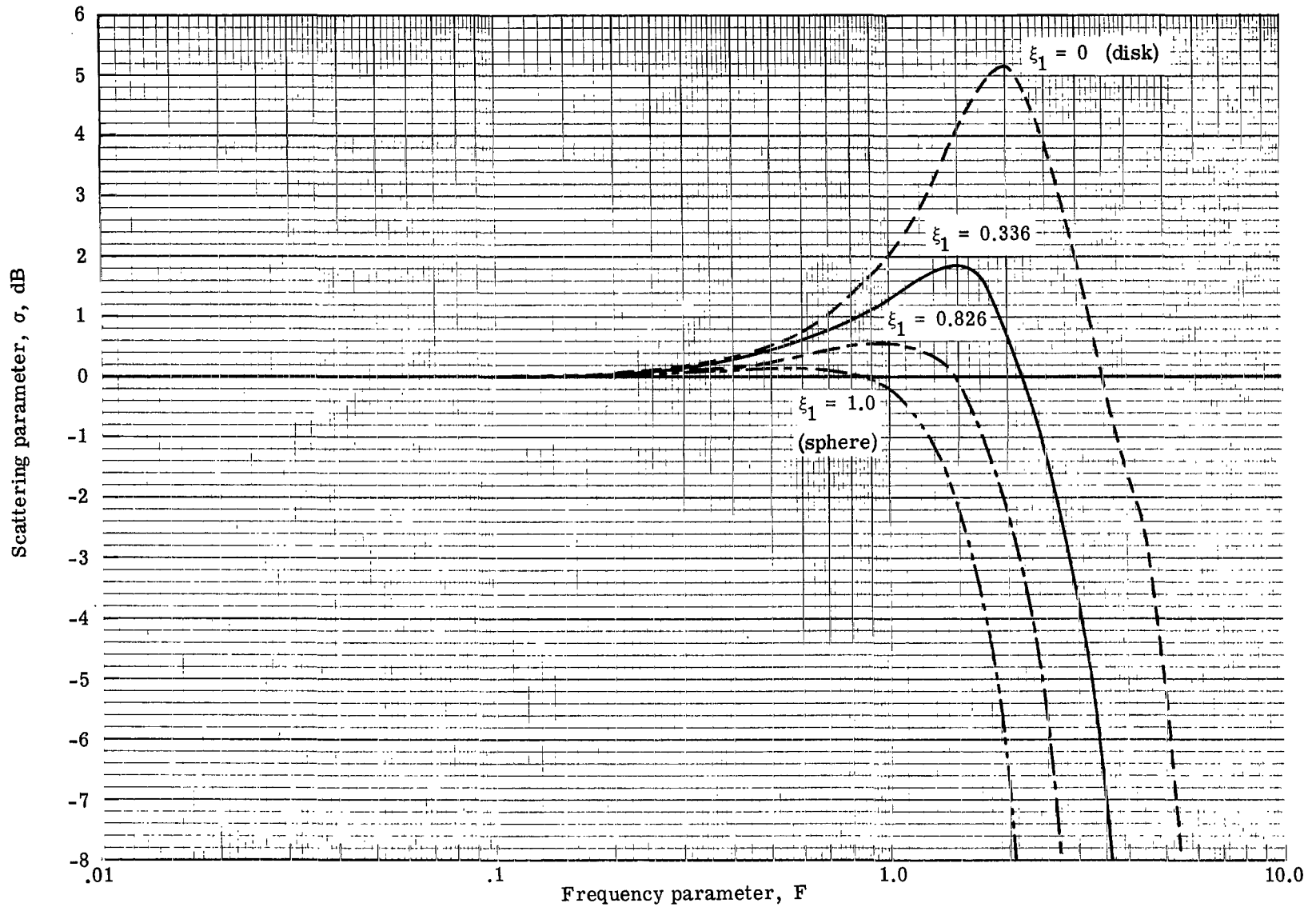
Figure 20.- Variation of scattering factor with frequency parameter for several geometric shapes.

*"The aeronautical and space activities of the United States shall be
conducted so as to contribute . . . to the expansion of human knowl-
edge of phenomena in the atmosphere and space. The Administration
shall provide for the widest practicable, and appropriate dissemination
of information concerning its activities and the results thereof."*
—NATIONAL AERONAUTICS AND SPACE ACT OF 1958

NASA SCIENTIFIC AND TECHNICAL PUBLICATIONS

TECHNICAL REPORTS: Scientific and
technical information considered important,
complete, and a lasting contribution to existing
knowledge.

TECHNICAL NOTES: Information less broad
in scope but nevertheless of importance as a
contribution to existing knowledge.

TECHNICAL MEMORANDUMS:
Information receiving limited distribution
because of preliminary data, security classifica-
tion, or other reasons. Also includes conference
proceedings with either limited or unlimited
distribution.

CONTRACTOR REPORTS: Scientific and
technical information generated under a NASA
contract or grant and considered an important
contribution to existing knowledge.

TECHNICAL TRANSLATIONS: Information
published in a foreign language considered
to merit NASA distribution in English.

SPECIAL PUBLICATIONS: Information
derived from or of value to NASA activities.
Publications include final reports of major
projects, monographs, data compilations,
handbooks, sourcebooks, and special
bibliographies.

TECHNOLOGY UTILIZATION
PUBLICATIONS: Information on technology
used by NASA that may be of particular
interest in commercial and other non-aerospace
applications. Publications include Tech Briefs,
Technology Utilization Reports and
Technology Surveys.

Details on the availability of these publications may be obtained from:

SCIENTIFIC AND TECHNICAL INFORMATION OFFICE

NATIONAL AERONAUTICS AND SPACE ADMINISTRATION
Washington, D.C. 20546